Plant, Cell & Environment

Plant, Cell and Environment (2014) **37**, 1299–1320 doi: 10.1111/pce.12234

Original Article

Differential cadmium and zinc distribution in relation to their physiological impact in the leaves of the accumulating *Zygophyllum fabago* L.

Isabelle Lefèvre[1], Katarina Vogel-Mikuš[2], Luka Jeromel[3], Primož Vavpetič[3], Sébastien Planchon[4], Iztok Arčon[3,5], Johannes T. Van Elteren[6], Gilles Lepoint[7], Sylvie Gobert[7], Jenny Renaut[4], Primož Pelicon[3] & Stanley Lutts[1]

[1]Groupe de Recherche en Physiologie végétale (GRPV), Earth and Life Institute – Agronomy (ELI-A), Université catholique de Louvain, Croix du Sud 4-5, bte L7.07.13, 1348 Louvain-la-Neuve, Belgium, [2]Department of Biology, Biotechnical Faculty, University of Ljubljana, Večna pot 111, 1000 Ljubljana, Slovenia, [3]Jožef Stefan Institute, Jamova 39, 1000 Ljubljana, Slovenia, [4]Department of Environment and Agrobiotechnologies (EVA), Centre de Recherche Public-Gabriel Lippmann, 41 rue du Brill, 4422 Belvaux, Luxembourg, [5]University of Nova Gorica, Vipavska 13, 5000 Nova Gorica, Slovenia, [6]Analytical Chemistry Laboratory, National Institute of Chemistry, Hajdrihova 19, 1000 Ljubljana, Slovenia and [7]Laboratory of Oceanology, MARE Centre, University of Liège, Sart Tilman B6c, 4000 Liège, Belgium

ABSTRACT

Cadmium and zinc share many similar physiochemical properties, but their compartmentation, complexation and impact on other mineral element distribution in plant tissues may drastically differ. In this study, we address the impact of 10 μM Cd or 50 μM Zn treatments on ion distribution in leaves of a metallicolous population of the non-hyperaccumulating species *Zygophyllum fabago* at tissue and cell level, and the consequences on the plant response through a combined physiological, proteomic and metabolite approach. Micro-proton-induced X-ray emission and laser ablation inductively coupled mass spectrometry analyses indicated hot spots of Cd concentrations in the vicinity of vascular bundles in response to Cd treatment, essentially bound to S-containing compounds as revealed by extended X-ray absorption fine structure and non-protein thiol compounds analyses. A preferential accumulation of Zn occurred in vascular bundle and spongy mesophyll in response to Zn treatment, and was mainly bound to O/N-ligands. Leaf proteomics and physiological status evidenced a protection of photosynthetically active tissues and the maintenance of cell turgor through specific distribution and complexation of toxic ions, reallocation of some essential elements, synthesis of proteins involved in photosynthetic apparatus or C-metabolism, and metabolite synthesis with some specificities regarding the considered heavy metal treatment.

Key-words: carbohydrates; EXAFS; heavy metals; LA-ICP-MS; micro-PIXE; photosynthetic-related parameters; plant proteomics; non-protein thiols; proline; water relations.

INTRODUCTION

Zinc and cadmium are two largely widespread pollutants of major environmental concern, originating mainly from mining activities, numerous industrial processes and as by-products of phosphatic fertilizer production (Alloway & Steinnes 1999; Kabata-Pendias & Pendias 2001; Nagajyoti *et al*. 2010). While Cd belongs to class B metals that fall under the category of non-essential trace elements, Zn plays essential metabolic roles in plants. This element is notably a structural component of a variety of metalloenzymes like carbonic anhydrase, alcohol dehydrogenase, Cu–Zn superoxide dismutase and RNA polymerase, but is furthermore required for the activity of a wide range of other enzymatic proteins such as dehydrogenases, aldolases, isomerases, transphosphorylases, RNA and DNA polymerase, and is also required for the synthesis of tryptophan (Marschner 1995; Kabata-Pendias & Pendias 2001; Broadley *et al*. 2007). Zinc thus plays an important role in regulating nitrogen metabolism, cell multiplication, photosynthesis and in the synthesis of nucleic acid, carbohydrates, proteins and auxins. However, above the plant requirements, this element becomes toxic. Despite the fact that Zn phytotoxicity is reported relatively often, especially for acidic and sludge soils (Kabata-Pendias & Pendias 2001), literature concerning mechanisms involved in its toxicity at cell and molecular level remains limited.

Both Cd and Zn can affect plant physiology causing stunted growth, root damage and chlorosis through a reduction of water uptake and water use efficiency, a nutritional imbalance and an oxidative stress (Poschenrieder & Barceló 1999; Lefèvre *et al*. 2010a; Nagajyoti *et al*. 2010; Gallego *et al*. 2012; Remans *et al*. 2012) leading to an impairment in respiration, photosynthesis, leaf chlorophyll stability, altered enzyme structure and activities, disruption in membrane integrity and lipid peroxidation (Monnet *et al*. 2001; Cherif *et al*. 2010; Nagajyoti *et al*. 2010).

Recently, several quantitative proteomic analyses have been devoted to the impact of Cd on various plant species as recently reviewed by Ahsan *et al*. (2009) and Villiers *et al*. (2011), which support and complement the Cd effects already observed through physiological and biochemical analyses.

Correspondence: S. Lutts. E-mail: stanley.lutts@uclouvain.be

These studies evidenced that the photosynthetic apparatus was severely disrupted under Cd toxicity, notably through the degradation or fragmentation of Rubisco (ribulose 1,5-bisphosphate carboxylase/oxygenase). A disorganization of photosystem I (PSI) was observed and various enzymes involved in the Calvin cycle and in the electron transfer chain (Cyt B6-f complex iron-sulphur subunit, chloroplast-$NADP^+$ oxidoreductase, oxygen-evolving enhancer protein 1 and 2) were down-regulated. These effects have direct consequences on the carbohydrate metabolism, as shown by Kieffer *et al.* (2008, 2009) and induce an oxidative burst. To overcome these toxic effects, an up-regulation of enzymes involved in reactive oxygen species (ROS) detoxification have been evidenced, as well as proteins involved in protein folding and stabilization, and proteins which catalyse the conjugation of toxic elements with metabolites (Sarry *et al.* 2006; Semane *et al.* 2010; Hossain *et al.* 2012). However, proteomic studies related to the impact of Zn excess remain scarce (Farinati *et al.* 2009; Garcia *et al.* 2009; Yuan *et al.* 2009; Fukao *et al.* 2011; Zeng *et al.* 2011).

Heavy metal effects directly depend on their localization in the tissues and their coordination with ligands. Mechanistic insight urgently requires sound information to this respect. Nutritional imbalance has long been recorded in response to Cd and Zn toxicities. However, few studies focus on essential and non-essential element distribution at tissue and cell level, and mainly concern hyperaccumulators able to cope with Cd or As toxicity and displaying extremely specific physiological mechanisms for this purpose, which are not relevant from the vast majority of the plant kingdom (Küpper *et al.* 2000; Zhao *et al.* 2000; Isaure *et al.* 2006; Vogel-Mikuš *et al.* 2008a,b; Pongrac *et al.* 2010; Huguet *et al.* 2012). The use of *in situ* techniques such as micro-proton-induced X-ray emission (micro-PIXE) or laser ablation inductively coupled plasma-mass spectrometry (LA-ICP-MS) with good lateral resolution and high sensitivity, enables element localization down to tissue or even cell levels, compared with other techniques such as scanning electron microscopy combined with energy-dispersive X-ray spectroscopy (SEM-EDX; Lombi *et al.* 2011). Although numerous metabolites have been quantified in plant organs, only few studies on Zn and Cd coordination using X-ray absorption spectroscopy (XAS) have been reported (Isaure *et al.* 2006; Vogel-Mikuš *et al.* 2010a; Huguet *et al.* 2012). This technique, including extended X-ray absorption fine structure (EXAFS) and X-ray absorption near edge structure (XANES), yields information on the local environment of the investigated atoms in the sample without any alteration by chemical sample pretreatments (number and types of neighbouring atoms, including their distance from the selected atom), and chemical oxidation state and coordination geometry of elements in complexes, respectively (Lombi & Susini 2009; Vogel-Mikuš *et al.* 2010b). This information about Cd and Zn coordination are crucial for the interpretation of the metabolic response previously described, and cannot be disconnected from metal cellular and subcellular location.

Zygophyllum fabago L., a succulent perennial forming a compact multibranched shrub, has been shown to be frequently encountered on disturbed sites, including mining areas contaminated by several heavy metals. This species, as most species in the plant kingdom, is not a hyperaccumulating plant but was shown to be able to rapidly accumulate in shoots up to 280 mg kg^{-1} dry weight (DW) of Cd and 600 mg kg^{-1} DW of Zn, in response to the addition of 10 μM Cd or 100 μM Zn in nutrient solution (Lefèvre *et al.* 2005, 2010a). On mine tailings, while heavy metals are less bioavailable compared with our laboratory conditions, *Z. fabago* was shown to accumulate similar concentration of Zn than in nutrient solution, ranging from 530 mg kg^{-1} DW to 770 mg kg^{-1} DW in shoots depending on the soil properties, with a shoot/root ratio of 1 in field conditions (Conesa *et al.* 2006, 2007). An integrated study of the response of this species to Cd or Zn treatment through combined approaches focusing on ion distribution at tissue and cell level, physiology, proteomic and metabolite analysis may help to unravel the precise impacts of both heavy metal toxicity on photosynthesis-related parameters and the intensity of the responses in classical non-hyperaccumulating plants. Such an integrated study has never been performed to the best of our knowledge and thus constitutes the aim of the present work. Moreover, this study will compare plant response to the exposure to two metals applied at concentrations that induce similar level of growth reduction (Lefèvre *et al.* 2010a).

MATERIALS AND METHODS

Plant material and culture conditions

Seeds of the metallicolous population *Z. fabago* were collected from a contaminated site situated near the city of Mazarrón in the Southeast of Spain (37°35′N, 1°18′W) on 15 bushes. Soil samples were collected at the base of the sampled bushes and analysed by standard procedures (Page *et al.* 1982). The soil texture was 21.9% clay, 20.4% fine silt, 11.8% coarse silt, 21% fine sand and 20.9% coarse sand. The organic C concentration was 1% and pH (KCl) and pH (H_2O) were 7.67 and 7.77, respectively. The concentrations of nutrients and heavy metals in soil were (in mg kg^{-1} dry matter): 10 P, 367 K, 700 N, 1030 Mg, 1017 Na, 42197 Ca, 63.63 Cu, 1957 Zn, 1650 Pb, 25.27 Ni, 8.23 Cd and 21.63 Cr.

Back to the laboratory, the seeds were sown and seedlings were grown in a mixture of sand and compost under controlled environmental conditions as already described (Lefèvre *et al.* 2009). The 7-week-old plants were then transferred to hydroponic system: nine tanks of 50 L were filled with an aerated modified Hoagland solution (Lefèvre *et al.* 2009). Thirty seedlings per tank were placed in polystyrene plates floating on the solution, which was renewed every week and the pH adjusted to 6.00 ± 0.05. Three tanks per treatment were randomized. After a week of acclimation (plants at the three- or four-node stage), $CdCl_2$ or $ZnSO_4$ were added to the solution in order to reach a final concentration of 10 μM or 50 μM, respectively. These concentrations were chosen on the basis of previous experiments to get similar tolerance index between Cd and Zn treatments after 3 weeks of heavy metal exposure (Lefèvre *et al.* 2010a; Lefèvre & Lutts; unpublished results). The treatment was

maintained for 4 weeks on 90 plants per treatment. Harvests were performed every 2 weeks from the time of stress application until the end of the experiment.

Leaves from the 3rd and 4th node, which corresponded to the youngest leaves at the time of stress imposition, expanded during the time course of the experiment and will be hereafter designated as 'elongating leaves'. It takes 1 month for a considered leaf to reach its maximal area (Lefèvre & Lutts; unpublished results). Ten plants per treatment were kept until the end of the experiment for measurements of leaf area, photosynthesis, stomatal conductance, transpiration and water potential of elongating leaves. Elongating leaves were harvested from 24 plants to make up six pools of leaves from four plants for each treatment. This material was devoted to Cd and Zn quantification, water content, osmotic potential, carbon isotopic discrimination and protecting compounds measurements. Quantitative proteomic analysis of elongating leaves was performed after 14 d of treatment. On the remaining plants, element distribution and EXAFS in leaves were investigated at the end of the experiment.

Determination of heavy metal concentration

For Cd and Zn quantification on elongating leaves, 50 mg of dry matter were digested as previously described (Lefèvre *et al*. 2010a). Cadmium and Zn concentrations were determined by atomic absorption spectrophotometry (Varian SpectrAA-300, Palo Alto, CA, USA). ICP standard ARISTAR (BDH Prolabo, VWR International, Radnor, PA, USA) was used for calibration curves.

Sample preparation for micro-PIXE and laser ablation analyses

Elongating leaves were detached from intact plants, quickly washed in deionized water and sectioned with a razor blade to smaller pieces of ca. 2 mm × 5 mm. The pieces were immediately inserted into a 2 mm stainless steel needle and dipped into tissue-freezing medium (Jung, Leica, Germany) and rapidly frozen in liquid propane cooled by liquid nitrogen (Vogel-Mikuš *et al*. 2008b). Leaf pieces were sectioned at a thickness of 60 μm with a Leica CM3050 cryotome (Leica, Bensheim, Germany) as previously described (Vogel-Mikuš *et al*. 2008b). Dry leaf cross sections were mounted on the Al sample holder between two thin layers of Pioloform foil.

Micro-PIXE analysis

The measurements by micro-PIXE and data evaluation for the biological samples of intermediate thickness were performed at the micro-PIXE set-up at Jožef Stefan Institute (Slovenia) as previously described in detail (Vogel-Mikuš *et al*. 2008b). Simultaneously, an on–off axis scanning transmission ion microscopy (STIM) was performed to determine beam exit energy from the sample, related to the sample local areal density (Pallon *et al*. 2004). The proton dose was determined by a rotating in-beam chopper (Vogel-Mikuš *et al*. 2008b).

For the generation of the elemental images, dynamic analysis methods were used (Ryan 2000), which are an essential part of GeoPIXE II software package. For the evaluation of Cd concentrations, the Cd Kα line at 23.17 keV was used, as the Cd L lines overlaps with the pronounced Kα line of potassium (Vogel-Mikuš *et al*. 2008b). The calibration of the PIXE method was verified by the analysis of the multi-elemental standard reference materials NIST SRM 1573a (tomato leaves, homogenized powder, analysed in the form of a pressed pellet), NIST SRM 1107 (Naval Brass B, alloy) and NIST SRM 620 (Soda-Lime Flat Glass), as well as in the intercomparison with ICP-MS, neutron activation and Roentgen fluorescence method (Nečemer *et al*. 2008). The inter-calibration of PIXE and STIM was verified by thin mono-elemental metallic foils.

The concentrations of elements in specific tissues of interest were extracted from numeric concentration matrices generated by GeoPIXE II, by manually encircling the selected regions in particular elemental distribution map using the ImageJ programme (http://www.macbiophotonics.ca/imagej/). Leaf morphology was studied on freeze-dried leaf cross sections using visible and ultraviolet (UV) light microscope (AxioImager ZI Carl Zeiss, Göttingen, Germany). The visible light images shown in Figs 2 and 3 were obtained with an Axiocam MRc colour digital camera, using the AxioVision 4.1 software.

Laser ablation ICP-MS analysis

A quadrupole ICP-MS (Agilent 7500ce, Palo Alto, CA, USA) interfaced with a 213 nm Nd:YAG laser ablation system (New Wave Research UP 213, Fremont, CA, USA) was used to quantify ions in leaf cross sections. Laser ablation in line scanning mode was performed on the entire surface, combining multiple parallel line scans with no spacing left between line scans. To obtain square pixels in the final elemental maps, the laser beam diameter has to equal the scanning speed times of the total acquisition time. Ablation parameters were as follows: laser energy density, 9 or 6.5 J cm^{-2}; pulse rate, 10 or 20 Hz; beam diameter, 8 or 12 μm; line scan speed, 4 μm s^{-1}; total acquisition time, 2 or 1 s. The ablated material was transported to the ICP using helium as a carrier gas (0.95 L min^{-1}); argon was added as a make-up gas before the torch of the ICP. The ions formed in the ICP were extracted in the quadrupole mass spectrometer and separated according to their mass-to-charge ratios. The ICP-MS was set up in a time-resolved analysis mode, measuring one data point per spectral peak for the subsequent isotopes: ^{24}Mg, ^{31}P, ^{34}S, ^{39}K, ^{43}Ca, ^{65}Mn, ^{66}Zn, ^{111}Cd, ^{56}Fe (the sum of the individual isotope acquisition times equalled the total acquisition time). Measurement of the background gases (He/Ar mixture) served to establish a blank signal for all masses. Since no suitable matrix-matched standards were available for these samples (Lobinski *et al*. 2006), data are reported in counts per second (cps).

Preparation of total protein extract and 2D-DIGE

Protein extraction was carried out according to Renaut *et al*. (2008). The protein concentration was determined using a

quantification kit (2D Quant Kit, GE Healthcare Uppsala, Sweden) using bovine serum albumin (BSA) (2 mg mL^{-1}) as the standard. After extraction, proteins were used for a multiplexed analysis by fluorescence difference gel electrophoresis (DIGE).

Four independent biological replicates of leaf extracts were prepared and resolved by 2D-DIGE. Control and exposed leaf extract were labelled either with Cy3 or Cy5 fluorescent dyes, and an internal standard containing equal amounts of all samples analysed was labelled (240 pmol for 30 μg of proteins) with Cy2 fluorescent dye following the manufacturer's recommendations (GE Healthcare). Samples were incubated for 30 min on ice and in the dark, and reactions stopped by an excess of lysine for 10 min.

A total of 90 μg of protein sample containing 30 μg of Cy3- and Cy5-labelled samples was pooled together with 30 μg of Cy2-labelled internal standard and adjusted with rehydration buffer (7 M urea, 2 M thiourea, 4% w/v CHAPS, 2% w/v DTT and 2% v/v pH 3-10NL IPG buffer, 0.6% DeStreak reagent) to a final volume of 450 μL.

Samples were separated in the first dimension by isoelectric focusing (IEF) overnight at 20 °C using an IPGphor3 isoelectric focusing system (GE Healthcare) and 24 cm 3-10NL IPG strips (GE Healthcare) as already described (Renaut *et al*. 2008).

After IEF, IPG strips were equilibrated and rinsed with running buffer, and gels were run at 15 °C in the EttanDalt 12 system (GE Healthcare) at 2.5 W/gel for 18 h as described by Renaut *et al*. (2008). After electrophoresis, gels were scanned on a Typhoon 9400 Variable Mode Imager (GE Healthcare) and analysed with DeCyder 7.0 software (GE Healthcare). Cy2, Cy3 and Cy5 components in each gel were individually scanned using the optimal excitation/emission wavelength for each DIGE fluor (Cy2 488/520 nm; Cy3 532/580 nm; Cy5 633/670 nm) and 100 μm as pixel size. Spot detection and quantification for each gel were carried out in a DeCyder differential in-gel analysis (DIA) module and matched in the DeCyder biological variation analysis (BVA) module. Relative expression ratios and statistical data for each differentially expressed spot were obtained. The threshold of changed fold-ratio was set at an absolute value of 1.5 to consider the variation as significant (with a P-value < 0.05).

Protein identification by MS

Using DeCyder 7.0 software (GE Healthcare), a picking list was created to collect the proteins of interest using the robotic system (Ettan Spot Handling Workstation, GE Healthcare) and collected in 96-well plates. Spots have been washed/desalted, proteins have been digested and peptides extracted and spotted on MALDI target as described in Renaut *et al*. (2008). Proteins were identified by searching against the NCBI 'Viridiplantae' and a 'Viridiplantae' expressed sequence tags database generated from the databases using MASCOT (Matrix Science, http://www.matrixscience.com). A search tolerance of 0.1 mg g^{-1} was allowed for MS data, while a 0.5 Da error was tolerated for fragment ions spectra. The search parameters allowed for carboxyamidomethylation of cysteine and oxidation of methionine and tryptophan residues. Homology identification was retained with a probability set at 95%.

Determination of leaf area, photosynthesis, chlorophyll fluorescence and pigment concentrations

The leaf area of elongating leaves was measured after 14 and 28 d of treatment by the analysis of a scanned leaf print with the Java image processing program ImageJ 1.34 (2005).

Gas exchange was recorded with a portable Infra Red Gas Analyser (Type LCA4, ADC BioScientific Ltd, Hoddesdon, UK) using a PLC Parkinson leaf cuvette on an intact leaf for 1 min (20 records min^{-1}) and an air flow of 300 mL min^{-1}. The instantaneous CO_2 assimilation rate (A) in CO_2 saturating condition, transpiration rate (E) and stomatal conductance (g_l) were determined on a leaf portion of 6.25 cm^2 of elongating leaves. Measurements were performed around midday (between 1100 h and 1400 h). The leaf temperature in the cuvette during measurements was set to 25–28 °C.

The stomatal density was measured by counting the number of stomata per unit of leaf area after measuring gas exchange. Clear nail polish was used to make prints of areas on the leaf abaxial face that were not heavily veined. The number of stomata and epidermal cells were counted on four areas of 0.265 mm × 0.265 mm per leaf to determine the stomatal and epidermal pavement cell density. The stomatal index [SI (%)] was calculated using the following equation (Salisbury 1927): $SI = SD/(ED + SD) \times 100$, where SD is stomatal density and ED is the density of epidermal pavement cells.

Chlorophyll fluorescence measurements were carried out *in situ* using a PEA fluorimeter (Hansatech, England) under a 15 s continuous light exposure provided by actinic light of 680 nm at 1500 μmol m^{-2} s. The recordings were performed on the middle part of the adaxial face of the leaves. A leaf portion was acclimated to darkness for 30 min. The maximal quantum yield of photochemistry (F_v/F_m) and the efficiency of electron transfer to the photosystem II (PSII) reaction centre (F_v/F_0) were measured.

Chlorophyll (Chl *a* and Chl *b*) and total carotenoid (xantophylls + β-carotene) concentrations were quantified on elongating leaves as already described by Lichtenthaler (1987).

Determination of plant water status

Samples of elongating leaves were weighed and dried in an oven for 72 h at 70 °C. The water content (WC) was determined as $WC = [(FW - DW)/FW] \times 100$.

Osmotic potential (Ψs) was quantified with a vapour pressure osmometer (Model 5500, Wescor, Logan, UT, USA) for elongating leaves according to Lefèvre *et al*. (2001). Osmotic potential was adjusted to the WC of the control plants according to Bajji *et al*. (1998): $\Psi s_{cor} = \Psi s \times (WC_{treated}/WC_{control})$ where the $WC_{treated}$ corresponds to the WC of Cd- or Zn-treated plants and $WC_{control}$ corresponds to the WC of control plants.

Leaf water potential (Ψw) was quantified on leaf disc with a HR33T Dew Point Microvoltometer (Wescor) connected to a C-52 sample chamber.

Carbon isotope discrimination

Samples of elongating leaves collected after 2 and 4 weeks of treatment were immediately oven-dried for 72 h at 70 °C. Approximately 5 mg of tissue for each sample were then ground to a fine powder. Isotopic and elemental measurements were performed using Optima mass spectrometer (Micromass, Manchester, UK) coupled to a C-N-S elemental analyser (Carlo Erba, Cornaredo, Italy). The C concentration is expressed in percent relative to the total DW. The reference material used was IAEA CH-6 ($\delta^{13}C = -10.4 \pm 0.2‰$). Carbon isotope composition ($\delta^{13}C$) values were obtained in part per thousand (‰) relative to Vienna Pee Dee Belemnite (vPDB) according to the following formula: $\delta^{13}C = [(R_{sample}/R_{standard}) - 1] \times 10^3$ where $R = {}^{13}C/{}^{12}C$. Carbon isotope discrimination ($\Delta^{13}C$) was calculated according to the formula of Hubick *et al.* (1986): $\Delta^{13}C = [(\delta_a - \delta_p)/(1 + \delta_p)] \times 10^3$ where δ_p is the $\delta^{13}C$ of the leaf sample and δ_a is the $\delta^{13}C$ of the atmospheric CO_2 (−8‰).

EXAFS measurement and data analysis

After harvest, elongating leaves were frozen in liquid nitrogen, freeze-dried for 2 d at −80 °C and at a pressure of 0.010 mbar (Alpha 2–4 LSC, Martin Christ Gefriertrocknungsanlagen GmbH, Osterode am Harz, Germany), homogenized in a mortar and packed in specially designed 9-cm-long plastic holders for Cd K-edge EXAFS or pressed in homogeneous pellets for Zn K-edge EXAFS.

The measurements were carried out at the beamline BM29 of the European Synchrotron Radiation Facility (ESRF, Grenoble, France), in transmission detection mode at room temperature. In all cases, the optimal total absorption thickness of at least 2 above the investigated absorption edge was obtained, with Cd and Zn edge jumps in the range of 0.1–1.5 depending on the concentration of the metal, determined in advance by SAA. In addition, EXAFS and XANES spectra of some reference Cd and Zn compounds with known metal valence states and structure, prepared in the form of homogenous self-standing pellets, were also recorded for comparison. The freeze-dried samples were chosen for XAS experiments instead of the samples in a frozen hydrated state, to improve the signal-to-noise ratio in the absorption spectra. Isaure *et al.* (2006) have reported that Cd speciation in plant tissues of non-hyperaccumulating plants is not significantly altered by the freeze-drying procedure. As only a very small fraction of the cellular metal is expected to exist in the form of free hydrated ions (Callahan *et al.* 2006), the freeze-drying procedure has been assumed not to drastically influence Cd and Zn ligand environment in the tissues of *Z. fabago*. The BM29 station of the ESRF was equipped with a Si 311 two-crystal monochromator with 2 eV resolution in the region of the Cd K-edge (26 711 eV) and about 1 eV resolution in the region of Zn K-edge (9659 eV). Higher harmonics of the beam were eliminated by a flat Pt coated mirror placed after the monochromator for the Cd K-edge experiment, and by a flat Si coated mirror for the Zn K-edge experiment. The intensity of the monochromatized beam was monitored with three ionization detectors, filled with krypton to a pressure of 120 mbar, 420 mbar and 450 mbar, respectively, for the Cd K-edge measurements. In the case of Zn K-edge measurements, the cells were filled with argon to a pressure of 60 mbar, 310 mbar and 310 mbar, respectively. In all cases, He was added, to a total pressure of 2 bars. Samples were placed between the first pair of detectors, and the reference metal foils between the posterior pair to check the stability of the energy scale. The absorption spectra were measured within the interval [−250 to 1000 eV] relative to the investigated absorption edge. In the XANES region, equidistant energy steps of 0.5 eV were used, while for the EXAFS region, equidistant k-steps ($\Delta k \approx 0.03$ Å^{-1}) were adopted, with an integration time of 1 s per step. The absorption spectra of three identical runs were superimposed to improve the signal-to-noise ratio and to check the stability and reproducibility of the detection system.

Extraction and analysis of organic compounds

For total acid soluble non-protein thiol (TAST) quantification in elongating leaves, 150 mg of frozen samples were ground in liquid nitrogen to a fine powder and then extracted according to Vromman *et al.* (2011) using Ellman's reagent. The absorbance at 412 nm was recorded after 2 min. The increase in absorbance was corrected for the absorbance of 2,4-dinitrothiocyanatobenzene (DNTB). Results were expressed as μmol of reduced glutathione (GSH) equivalents per g of fresh weight (FW) from a GSH standard concentration curve. The recovery and oxidation of acid-soluble thiols were determined using GSH as an external and internal standard.

For total soluble sugar quantification in elongating leaves, 350 mg of frozen samples were ground in liquid nitrogen to a fine powder and then extracted with 7 mL of 70% ethanol. Extracts were centrifuged at 6600 *g* for 10 min. The total soluble sugar concentration in the supernatant was estimated using the anthrone reagent method according to Yemm & Willis (1954).

For free proline quantification in leaves, 100 mg of FW were ground in liquid nitrogen to a fine powder and then extracted with 10 mL of salicylic acid 3% (v/v) in boiled water during 30 min and then cooled on ice; after centrifugation at 5000 *g*, supernatant was filtered on filter paper (Whatman®, 11 μm; GE Healthcare Whatman plc, Maidstone, Kent, UK). Free proline was specifically quantified using ninhydrine acid reagent according to Bates *et al.* (1973).

Statistical analysis

The experiment was repeated twice, and led to statistical similar results. Normality tests were performed and further transformations of the raw data were performed when required. An analysis of variance was performed on the mineral element concentration, organic metabolite

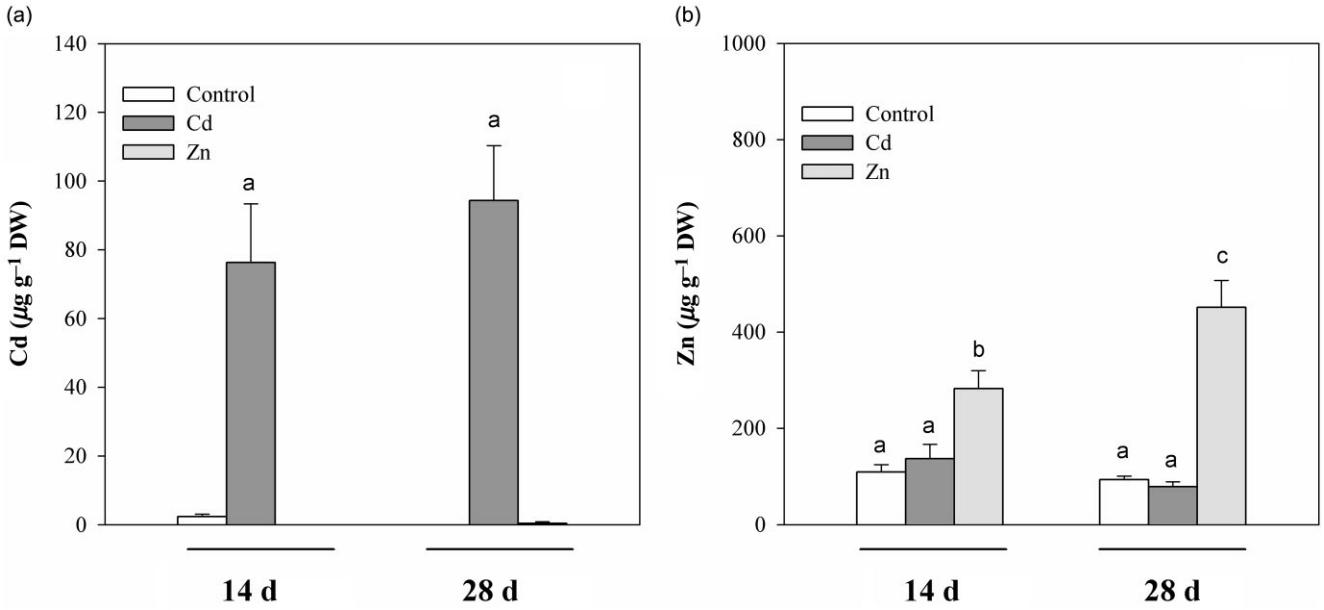

Figure 1. Cd (a) and Zn (b) concentration in the leaves of *Zygophyllum fabago* in the absence (control) or in the presence of 10 μM Cd or 50 μM Zn after 14 and 28 d of treatment. Values are based on the mean of six replicates, vertical bars are SE. For each of the parameters, histograms showing the same letter are not significantly different at $P < 0.05$ level.

concentration, and photosynthesis- and water-status-related parameters using the PROC GLM procedure in the SAS software (SAS 9.1 System for Windows, SAS Institute Inc., Cary, NC, USA) using variance analysis with two cross-fixed factors (treatment × duration of treatment). One-way ANOVA tests were also carried out for each organ, with treatment or duration of treatment as the main factor. Differences between means have been analysed with a Scheffé test with a confidence limit of 95%.

Distribution of mineral elements has been analysed by a one-way ANOVA test using the PROC GLM procedure in the SAS software with tissues as the main factor. Quantitative and qualitative co-localization analysis of elements intensities was determined on the larger maps of leaf cross sections (from 2000 μm × 2000 μm to 500 μm × 500 μm), employing ImageJ software with the 'intensity correlation analysis' plug-in, generating Pearson's correlation coefficients (r), Mander's overlap coefficients (R) and Intensity Correlation Quotients (ICQ) (http://www.macbiophotonics.ca/imagej/colour_analysis.htm). Values for the Pearson's correlation coefficients range from 1 to −1, where a value of 1 represents perfect correlation, a value of −1 represents perfect exclusion and zero represents random localization. The Mander's overlap coefficients ranges between 1 and 0, with 1 representing high co localization and 0 representing no co localization. The ICQ values are distributed between −0.5 and +0.5, with random staining represented by ICQ~0, segregated staining by $0 > ICQ \geq -0.5$ and dependent staining by $0 < ICQ \leq +0.5$ (Li *et al.* 2004).

For the analysis of the relative abundance of proteins, only statistically significant results were considered (Student t-test $P < 0.05$, with treated/control or Cd/Zn as factor). Differentially expressed proteins with an absolute ratio of at least 1.5-fold were selected. The analysis was performed using DeCyder 7.0 software (GE Healthcare).

RESULTS

Element concentration and distribution within leaf tissues

Only 16.7% of the Cd-treated plants died during the course of the experiment, while no mortality occurred in response to Zn treatment. Cadmium concentration increased in leaves of Cd-treated plants during the first 14 d and then remained constant (Fig. 1a). A progressive and significant increase in Zn concentration was observed in elongating leaves in response to Zn treatment (Fig. 1b).

Figure 2 (obtained by micro-PIXE analysis) and Fig. 3 (obtained by LA-ICP-MS analysis) show a representative example of element distribution in a leaf cross section of *Z. fabago* treated with 50 μM Zn and 10 μM Cd, respectively. Element distribution maps obtained by micro-PIXE and LA-ICP-MS techniques showed similar results in terms of element distribution. In response to Cd treatment, Cd concentrations in the non-hyperaccumulating species were at the threshold of detection for this element and did not provide satisfactory statistic. In this way, the use of LA-ICP-MS allowed the acquisition of qualitative information about Cd distribution. The Cd map obtained with this technique suggests a quite homogeneous distribution of Cd within the leaf cross section with few hot spots located near vascular bundles (Fig. 3).

To precisely analyse the element distribution obtained through micro-PIXE measurements (Fe, Mn, Zn, Ca, Cl, K, Mg, Na, P and S), seven distinct anatomical areas were distinguished in the leaves of *Z. fabago*, namely, the upper and

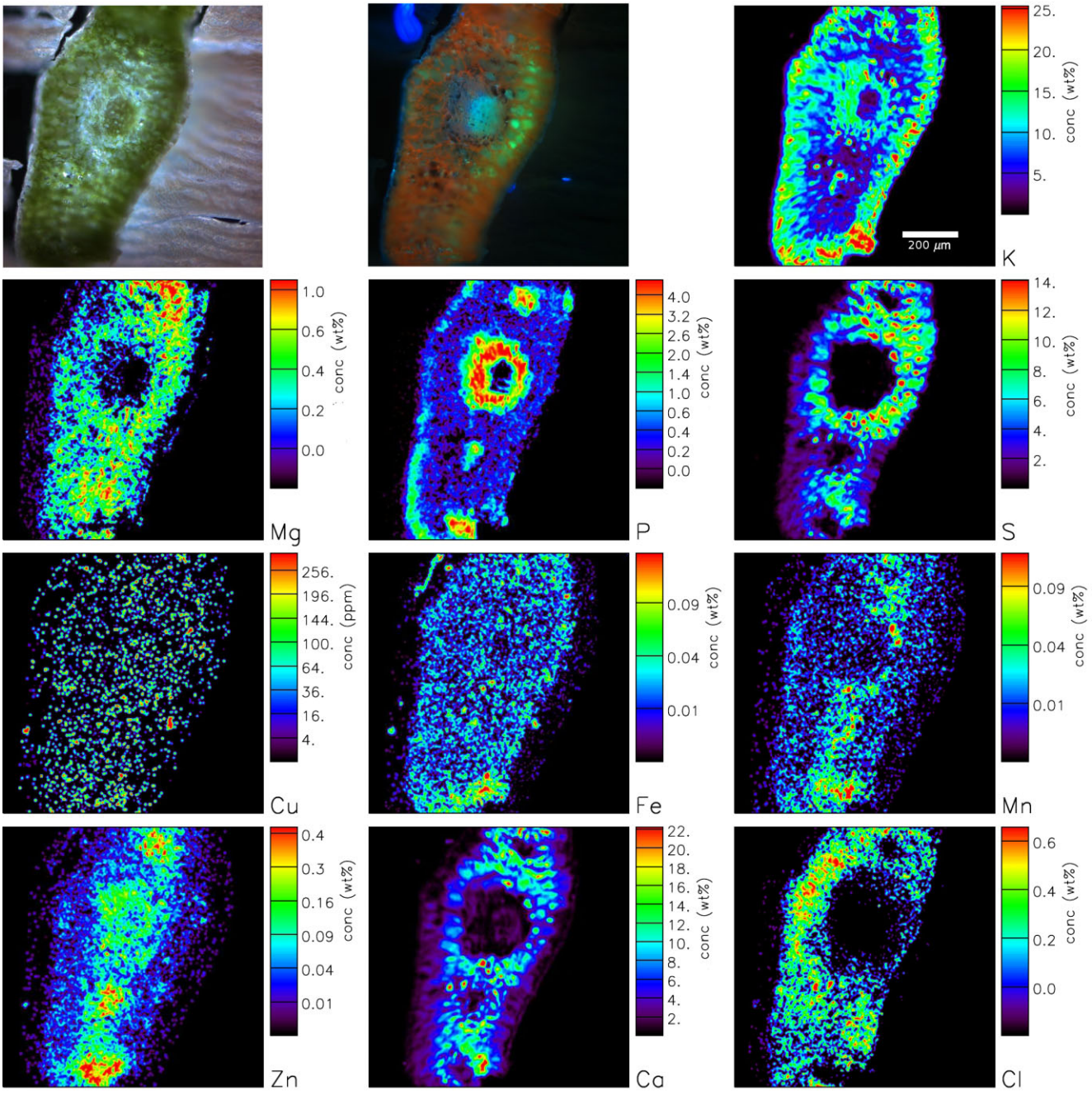

Figure 2. Photographs of a representative leaf cross section of *Zygophyllum fabago* treated with 50 μM Zn during 4 weeks as analysed by light microscopy (upper left), visible light and ultraviolet (UV) light source excitation (from left to right, respectively), and the associated quantitative elemental maps of K, Mg, P, S, Cu, Fe, Mn, Zn, Ca and Cl generated with GEOPIXE II software package after micro-PIXE analysis. Scan size, 1000 μm × 1000 μm.

lower epidermis, the palisade and spongy mesophyll, and the vascular bundle with upper and lower midrib parenchyma (Table 1). The vascular bundle was also subdivided into xylem, phloem and sclerenchyma. In control plants, the highest concentrations of Mn, Ca, Cl, Mg and S were found in mesophyll, while K and P were mainly found in epidermal layers and the vascular bundle, especially in phloem. Zinc was mainly found in spongy mesophyll, phloem and sclerenchyma. Iron was more homogeneously distributed within tissues, the highest concentrations being found in mesophyll and the vascular bundle. The highest concentration of Cu was located in palisade mesophyll and the xylem region.

The Cd treatment induced a significant increase of K in palisade mesophyll ($P = 0.0050$), xylem ($P = 0.0259$), phloem ($P = 0.0067$) and sclerenchyma ($P = 0.0011$; Table 1). A significant decrease in the Ca concentration was observed in

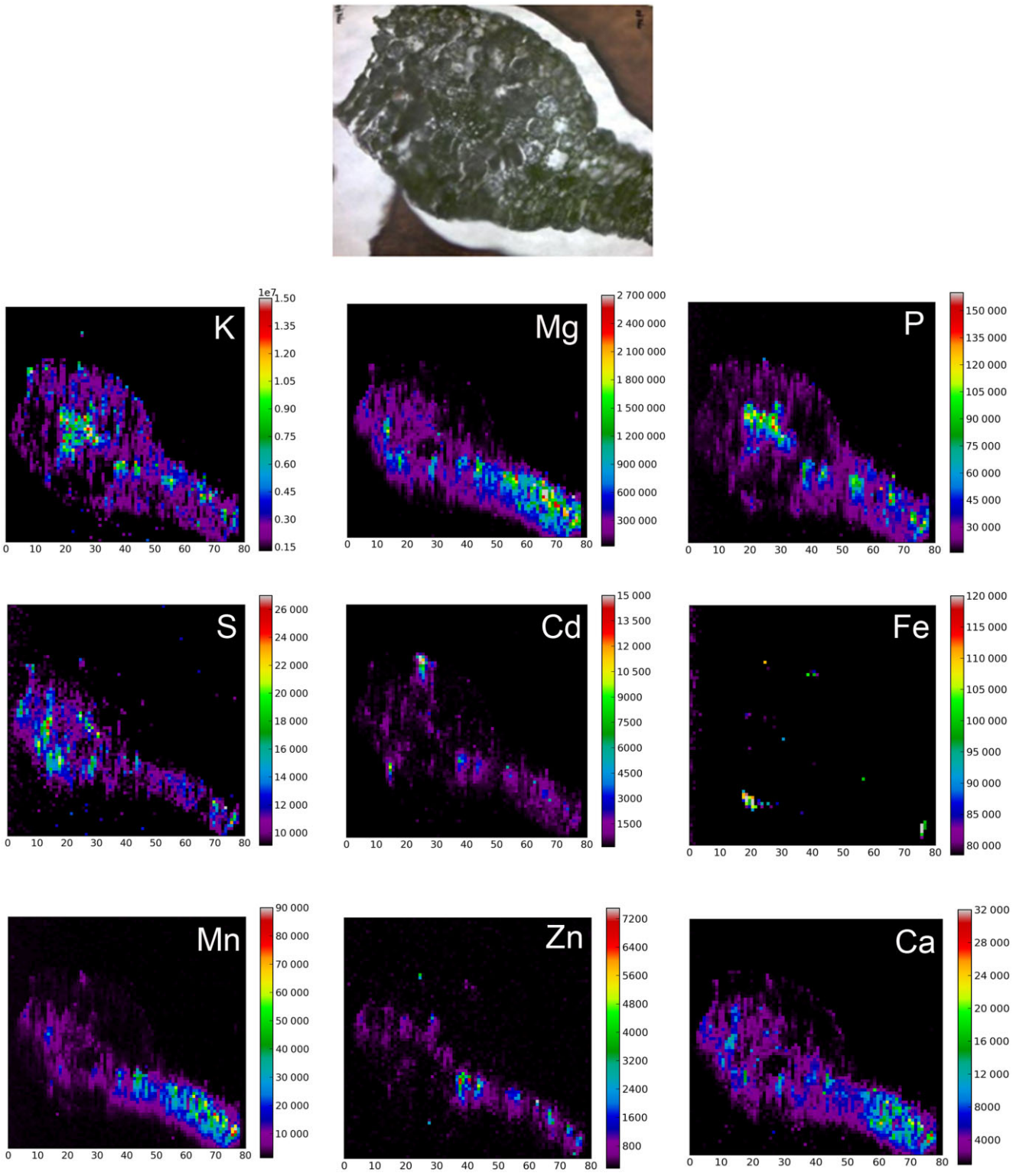

Figure 3. Photographs of a representative leaf cross section of *Zygophyllum fabago* treated with 10 μM Cd during 4 weeks as analysed by light microscopy (top), visible light source excitation, and the associated qualitative elemental maps of K, Mg, P, S, Cd, Fe, Mn, Zn, and Ca obtained through LA-ICP-MS analysis. Elemental densities (in counts per second) are visualized as jet colours with lower image densities mapped onto 'cool' colours and higher densities onto 'hot' colours.

Table 1. Micro-PIXE localization of elements within leaf cross section of *Zygophyllum fabago* in the absence (control) or in the presence of 10 μM Cd or Zn μM Zn after 28 d of treatment

Element	Control	Cd	Zn	Control	Cd	Zn	Control	Cd	Zn
	Upper epidermis 			Palissade mesophyll 			Spongy mesophyll 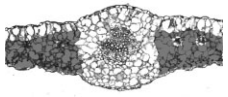		
Macro-elements (mg g^{-1} DW)									
Ca	22.8 ± 3.6 Da	21.2 ± 5.4 Ba	12.6 ± 1.8 Ca	**140.5 ± 10.7 Aa**	**62.3 ± 12.0 ABb**	**45.4 ± 4.0 ABb**	**102.1 ± 10.1 CDa**	**61.1 ± 14.7 ABb**	**66.4 ± 7.2 Aab**
K	59.5 ± 7.6 ABa	97.3 ± 10.0 BCa	83.4 ± 25.5 Aa	**20.0 ± 3.1 Bb**	**75.2 ± 12.3 BCa**	**74.9 ± 18.8 Aa**	20.7 ± 1.2 Ba	51.9 ± 10.3 Ca	43.5 ± 12.4 Aa
Mg	5.9 ± 1.5 Aa	3.8 ± 0.9 Ba	2.4 ± 0.9 Aa	11.3 ± 2.5 Aa	5.6 ± 1.1 ABa	5.7 ± 3.0 Aa	11.9 ± 1.4 Aa	7.9 ± 2.1 ABa	5.9 ± 2.8 Aa
P	**22.5 ± 2.5 ABa**	**4.3 ± 1.7 Bb**	**8.3 ± 3.8 ABCb**	7.2 ± 2.1 BCa	3.6 ± 0.5 Ba	5.3 ± 0.5 ABCa	4.5 ± 0.6 Ca	4.1 ± 0.2 Ba	3.9 ± 0.4 BCa
S	10.1 ± 0.7 Ca	12.8 ± 1.9 Ba	9.9 ± 2.4 ABa	**65.3 ± 7.9 ABa**	**38.0 ± 3.2 Bb**	**35.6 ± 8.0 ABb**	40.5 ± 3.1 BCa	36.5 ± 7.5 Ba	31.6 ± 5.2 ABa
Micro-elements (μg g^{-1} DW)									
Cu	26 ± 3 Aa	31 ± 7 Ba	28 ± 12 Aa	72 ± 3 Aa	52 ± 17 ABa	31 ± 8 Aa	42.48 ± 2.61 Aa	43 ± 21 ABa	41 ± 14 Aa
Cd	–	<LOD	–	–	<LOD	–	–	<LOD	–
Fe	112 ± 19 ABa	130 ± 20 ABa	149 ± 48 Aa	240 ± 46 ABa	186 ± 39 ABa	192 ± 36 Aa	188 ± 41 ABa	212 ± 63 ABa	147 ± 15 Aa
Mn	67 ± 16 Ba	63 ± 11 Ba	73 ± 20 ABa	**246 ± 41 Aa**	**112 ± 25 ABb**	**149 ± 32 ABab**	164 ± 30 ABa	166 ± 68 ABa	201 ± 47 Aa
Zn	**59 ± 8 Bb**	**44 ± 8 Bb**	**112 ± 19 Ca**	**86 ± 9 ABb**	**63 ± 16 Bb**	**333 ± 62 BCa**	**101 ± 12 ABb**	**91 ± 30 Bb**	**578 ± 69 ABa**
Cl	13 637 ± 1890 ABa	8620 ± 6948 Ba	3696 ± 1256 Aa	21 172 ± 5094 ABa	9717 ± 8182 Ba	5235 ± 2194 Aa	20 427 ± 4172 ABa	11 962 ± 9744 Ba	5523 ± 2649 Aa
	Lower epidermis 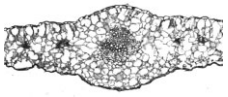			Upper midrib parenchyma 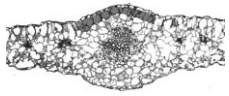			Lower midrib parenchyma 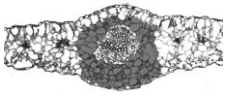		
Macro-elements (mg g^{-1} DW)									
Ca	20.8 ± 2.3 Da	11.0 ± 3.5 Ba	15.3 ± 4.8 BCa	**60.5 ± 5.4 BCb**	**133.3 ± 12.9 Aa**	**34.0 ± 9.5 ABCb**	26.6 ± 7.3 CDa	42.2 ± 7.4 Ba	37.1 ± 2.3 ABCa
K	63.7 ± 9.6 ABa	95.5 ± 17.8 BCa	73.4 ± 12.9 Aa	**55.2 ± 2.9 ABb**	**46.7 ± 1.9 Cb**	**88.8 ± 16.3 Aa**	**64.3 ± 7.3 ABb**	**208.3 ± 59.8 Aa**	**76.6 ± 4.6 Ab**
Mg	5.0 ± 0.7 Aa	4.0 ± 1.5 Ba	1.5 ± 0.1 Aa	**8.5 ± 3.0 Aab**	**13.6 ± 2.3 Aa**	**2.7 ± 1.0 Ab**	4.4 ± 1.7 Aa	7.7 ± 4.9 ABa	1.9 ± 0.1 Aa
P	17.2 ± 2.6 ABCa	9.0 ± 5.0 ABa	7.1 ± 1.0 ABCa	5.4 ± 1.8 Ca	6.2 ± 1.2 Ba	3.3 ± 0.6 Ca	4.0 ± 2.0 Ca	10.4 ± 7.1 ABa	3.2 ± 0.2 Ca
S	15.4 ± 2.4 Ca	10.2 ± 1.8 Ba	9.5 ± 5.8 ABa	**81.9 ± 9.0 Aab**	**117. ± 10.8 Aa**	**40.6 ± 12.8 Ab**	22.0 ± 5.2 Ca	45.4 ± 11.3 Ba	30.0 ± 2.8 ABa
Micro-elements (μg g^{-1} DW)									
Cu	n.d.	34 ± 17 Ba	108 ± 93 Aa	**68 ± 10 Aab**	**104 ± 11 ABa**	**30 ± 1 Ab**	**35 ± 5 Ab**	**105 ABa**	**24 ± 4 Ab**
Cd	–	< LOD	–	–	< LOD	–	–	< LOD	–
Fe	104 ± 10 Ba	115 ± 22 Ba	118 ± 28 Aa	166 ± 35 ABa	281 ± 61 ABa	216 ± 78 Aa	123 ± 5 ABa	547 ± 399 ABa	131 ± 37 Aa
Mn	57 ± 11 Ba	76 ± 32 Ba	65 ± 7 ABa	120 ± 23 ABa	248 ± 44 Aa	121 ± 28 ABa	87 ± 8 ABa	253 ± 131 Aa	73 ± 14 ABa
Zn	**72 ± 13 Bb**	**51 ± 15 Bb**	**188 ± 39 Ca**	**74 ± 8 ABb**	**84 ± 13 Bb**	**186 ± 30 Ca**	60 ± 20 Ba	136 ± 73 ABa	225 ± 17 Ca
Cl	18 914 ± 3021 ABa	8729 ± 6418 Ba	7021 ± 4195 Aa	**17 414 ± 1324 ABb**	**33 388 ± 3982 ABa**	**1724 ± 117 Ac**	**29414 ± 4771 Ab**	**84 662 ± 11587 Aa**	**3429 ± 498 Ac**
	Xylem 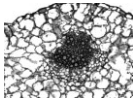			Phloem 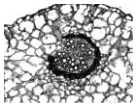			Sclerenchyma 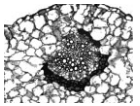		
Macro-elements (mg g^{-1} DW)									
Ca	**16.9 ± 1.0 Dab**	**23.3 ± 3.7 Ba**	**9.3 ± 0.1 Cb**	**12.9 ± 2.3 Db**	**30.0 ± 4.7 Ba**	**10.9 ± 1.8 Cb**	13.4 ± 1.9 Da	46.5 ± 15.8 Ba	16.8 ± 0.6 BCa
K	**51.4 ± 5.0 ABb**	**112.0 ± 17.5 BCa**	**53.6 ± 3.2 Aab**	**83.0 ± 9.6 Ab**	**155.3 ± 13.8 ABa**	**102.8 ± 4.2 Aab**	**66.7 ± 8.2 Ab**	**119.1 ± 6.2 ABCa**	**71.0 ± 7.8 Ab**
Mg	4.6 ± 2.3 Aa	6.2 ± 2.1 ABa	1.3 ± 0.2 Aa	5.6 ± 2.8 Aa	12.5 ± 4.0 ABa	3.4 ± 1.7 Aa	**4.4 ± 1.7 Aab**	**13.2 ± 2.4 Aa**	**2.8 ± 0.8 Ab**
P	12.1 ± 3.5 ABCa	17.4 ± 6.5 ABa	10.3 ± 0.9 ABCa	29.4 ± 2.3 Aa	34.0 ± 7.9 Aa	25.3 ± 6.4 Aa	9.4 ± 1.3 ABCa	8.7 ± 2.4 ABa	13.7 ± 3.9 ABCa
S	**6.7 ± 2.8 Cab**	**18.4 ± 3.1 Ba**	**4.8 ± 0.0 Bb**	**11.5 ± 2.2 Cb**	**34.4 ± 4.6 Ba**	**3.8 ± 2.3 Bb**	**16.7 ± 2.9 Cb**	**51.4 ± 15.4 Ba**	**13.1 ± 0.7 ABb**
Micro-elements (μg g^{-1} DW)									
Cu	**70 ± 12 Aab**	**163 ± 45 Aa**	**34 ± 2 Ab**	**53 ± 11 Ab**	**164 ± 7 Aa**	**35 ± 6 Ab**	**47 ± 10 Ab**	**118 ± 18 ABa**	**25 ± 4 Ab**
Cd	–	<LOD	–	–	<LOD	–	–	<LOD	–
Fe	234 ± 15 ABa	284 ± 89 ABa	78 ± 19 Aa	**265 ± 32 Bb**	**724 ± 178 Aa**	**198 ± 44 Ab**	**118 ± 15 ABb**	**309 ± 61 ABa**	**134 ± 13 Aab**
Mn	**72 ± 9 ABab**	**188 ± 40 ABa**	**35 ± 5 Bb**	**104 ± 18 ABb**	**254 ± 46 Aa**	**101 ± 34 ABb**	**77 ± 15 ABb**	**229 ± 36 ABa**	**94 ± 5 ABb**
Zn	**76 ± 8 ABb**	**92 ± 15 ABb**	**720 ± 40 ABa**	**145 ± 8 Ac**	**270 ± 34 Ab**	**768 ± 59 Aa**	**110 ± 22 ABb**	**75 ± 13 Bb**	**585 ± 87 ABa**
Cl	**8673 ± 2984 Bab**	**64 315 ± 26083 ABa**	**835 ± 13 Ab**	**10 780 ± 2138 ABb**	**73 103 ± 14298 ABa**	**2275 ± 1564 Ab**	**18 335 ± 1594 ABb**	**32 320 ± 3458 ABa**	**1711 ± 673 Ac**

Figures represent the leaf cross section with the darkened area corresponding to the different leaf structures from which the X-ray spectra were extracted and analysed. Values are in mg g^{-1} or μg g^{-1} DW. Values are the mean of at least five replicates ± SE. LOD, limit of detection of the measurement. In different tissues, values for the same element and for a similar treatment showing the same capital letter are not significantly different at $P < 0.05$ level. For the different treatments, values for the same element and for a similar tissue showing the same lower case letter are not significantly different at $P < 0.05$ level, and those which present significant differences are in bold.

Table 2. Micro-PIXE localization of elements within mesophyll cells of leaf cross section of *Zygophyllum fabago* in the absence (control) or in the presence of 10 μM Cd or 50 μM Zn after 28 d of treatment

	Mesophyll symplast 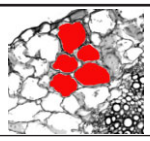			Mesophyll apoplast 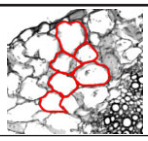		
Element	Control	Cd	Zn	Control	Cd	Zn
Macro-elements (mg g^{-1} DW)						
Ca	114.4 ± 35.7 Aa	131.6 ± 24.4 Aa	49.0 ± 11.6 Aa	**48.7 ± 12.2 Ab**	**102.7 ± 13.5 Aa**	**26.1 ± 2.4 Ab**
K	40.5 ± 5.7 Aa	92.2 ± 54.6 Aa	66.5 ± 13.4 Aa	44.3 ± 11.2 Aa	100.5 ± 39.0 Aa	64.7 ± 10.0 Aa
Mg	14.9 ± 3.0 Aa	12.8 ± 1.5 Aa	6.8 ± 3.5 Aa	**10.8 ± 1.3 Ab**	**22.4 ± 2.4 Ba**	**5.6 ± 2.3 Ab**
P	7.4 ± 1.3 Aa	7.8 ± 1.4 Aa	4.1 ± 0.5 Aa	7.6 ± 0.9 Aa	9.9 ± 2.4 Aa	5.8 ± 1.8 Aa
S	**92.4 ± 21.4 Aab**	**129.5 ± 19.7 Aa**	**40.5 ± 9.6 Ab**	**40.2 ± 8.2 Ab**	**84.5 ± 8.5 Aa**	**22.1 ± 3.6 Ab**
Micro-elements (μg g^{-1} DW)						
Cu	**74 ± 11 Aa**	**112 ± 11 Aa**	**29 ± 1 Ab**	**50 ± 12 Aab**	**87 ± 16 Aa**	**26 ± 4 Ab**
Cd	–	<LOD	–	–	<LOD	–
Fe	297 ± 83 Aa	343 ± 67 Aa	145 ± 15 Aa	**213 ± 32 Aab**	**448 ± 96 Aa**	**148 ± 17 Ab**
Mn	265 ± 84 Aa	304 ± 41 Aa	153 ± 63 Aa	**154 ± 32 Aa**	**329 ± 39 Aa**	**99 ± 29 Ab**
Zn	**80 ± 7 Ab**	**100 ± 23 Ab**	**401 ± 156 Aa**	**93 ± 13 Ab**	**106 ± 18 Ab**	**318 ± 85 Aa**
Cl	**17 529 ± 1773 Aa**	**37 640 ± 15753 Aa**	**2080 ± 176 Ab**	**20 440 ± 3564 Ab**	**62 190 ± 10417 Aa**	**2573 ± 338 Ac**

Figures represent the leaf cross section with the coloured area corresponding to the different leaf structures from which the X-ray spectra were extracted and analysed. Values are in mg g^{-1} or μg g^{-1} DW. Values are the mean of at least five replicates ± SE. LOD, limit of detection of the measurement. In different structures, values for the same element and for a similar treatment showing the same capital letter are not significantly different at $P < 0.05$ level. For the different treatments, values for the same element and for a similar structure showing the same lower case letter are not significantly different at $P < 0.05$ level, and those which present significant differences are in bold.

palisade mesophyll ($P < 0.0001$) and in spongy mesophyll ($P = 0.0499$), while an increase of the Ca element concentration occurred in the phloem region ($P = 0.0093$) and in upper midrib parenchyma located near the vascular bundle ($P = 0.0004$) compared with control plants. Phosphorus significantly decreased in the upper epidermis ($P = 0.0006$). Sulphur decreased in palisade mesophyll ($P = 0.0102$) while it increased in phloem and sclerenchyma ($P = 0.0014$ and $P = 0.0275$, respectively) in response to Cd treatment. Despite the fact that no significant variations were found, Mg tended to increase in phloem, sclerenchyma and palisade mesophyll located near vascular bundle in response to Cd. Chloride increased in the vascular bundle, more specifically in phloem ($P = 0.0013$) and sclerenchyma ($P < 0.0001$), and in the mesophyll region located in the vicinity of the vascular bundle, in both upper midrib ($P < 0.0001$) and lower midrib parenchyma ($P = 0.0013$). Regarding micro-elements, the Cu concentration increased in the region of vascular tissues, more specifically in phloem ($P < 0.0001$), sclerenchyma ($P = 0.0021$) and in mesophyll located in the vicinity of the vascular bundle, with a significant increase in lower midrib parenchyma ($P = 0.0064$; Table 1). A similar trend was observed for the Fe and Mn concentration in phloem ($P = 0.0285$ and $P = 0.0459$, respectively) and sclerenchyma ($P = 0.0275$ and $P = 0.0059$, respectively), while a significant decrease of the Mn concentration was observed in palisade mesophyll ($P < 0.0001$). The Zn concentration in phloem increased in response to Cd treatment compared with control plants ($P < 0.0001$).

In response to Zn treatment, the highest concentration increase of this element was observed in the spongy mesophyll and in the vascular bundle with an increase of 472% and 527%, respectively, compared with the control plants (Table 1). In the vascular bundle, the high concentration increase of Zn was mainly associated with the xylem region with an increase of 847% compared with the control plants. The potassium concentration was significantly increased in response to Zn excess, both in the palisade mesophyll and in the upper midrib parenchyma ($P = 0.0050$ and $P = 0.0123$, respectively). An opposite trend was observed for the Ca and S concentrations, more specifically related to a significant decrease in the palisade mesophyll ($P < 0.0001$ and $P = 0.0102$). Phosphorus significantly decreased in the upper epidermis ($P = 0.0006$).

Scanning from 330 μm × 330 μm to 165 μm × 165 μm leaf regions enabled us to distinguish between apoplast and symplast of mesophyll cells (Table 2, Supporting Information Fig. S1). In both control and Zn-treated plants, no significant differences were found in element concentration between symplast and apoplast of leaf mesophyll cells. However, a higher concentration of Mg was observed in apoplast compared with symplast in Cd-treated leaves ($P = 0.0095$). A strong accumulation of Zn was observed both in symplast and apoplast of leaf mesophyll from Zn-treated plants compared with those of control and Cd-treated plants. Both Cd and Zn treatments induced a redistribution of some essential elements; Cd induced an increase in S, Mg, Ca and Cl concentration in apoplast of mesophyll cells compared with the controls ($P = 0.0004$, $P = 0.0006$, $P = 0.0013$ and $P < 0.0001$, respectively) and Zn induced a decrease in Cl concentration in both symplast and apoplast ($P < 0.0001$) in Mn concentration in apoplast ($P = 0.0027$) and in Cu concentration in symplast mesophyll cells ($P = 0.0007$) compared with the controls. Some differences in element concentration

appeared significant between Cd and Zn treatment, indicating an opposite effect of these treatments on some elements; the Cu concentration was significantly higher in both symplast and apoplast of leaf mesophyll cell of Cd-treated plants than those of Zn-treated plants ($P = 0.0007$ and $P = 0.0245$, respectively), these differences in Cu concentration being related to a slight increase in response to Cd treatment and a strong decrease in response to Zn treatment compared with the controls. The concentration of Fe was higher in apoplast of leaf mesophyll cells of Cd-treated plants than in those of Zn-treated plants ($P = 0.0080$).

Intensity correlation analysis did not indicate clear co-localizations between Zn and other elements (Supporting Information Fig. S2). In response to all treatments, a co-localization was observed between Ca, Mg and S ($r > 0.482$, $R > 0.741$ and $ICQ > 0.175$ between Ca and Mg; $r > 0.748$, $R > 0.865$ and $ICQ > 0.285$ between Ca and S; $r > 0.408$, $R > 0.657$ and $ICQ > 0.160$ between Mg and S; Supporting Information Fig. S2).

Proteome analysis

The study focused on the spots in which intensity significantly changed between the treated plants and the controls or between Cd- and Zn-treated plants (threshold of changed fold-ratio set at an absolute value of 1.5 and P-value < 0.05). After 14 d of stress exposure, 53 out of 67 identified proteins, excluding spots wherein two proteins were identified, were involved in photosynthetic apparatus, carbohydrate and C-metabolism (Table 3). Only three proteins were involved in antioxidant defence and detoxification. Out of the 67 identified proteins, only 13 spots changed significantly in their intensity between Cd- and Zn-treated plants, indicating some similarities in the regulation of most of the proteins of interest, despite an abundance which significantly differ from the control plants.

Out of the photosynthetic apparatus-related proteins, 2 chlorophyll *a*/*b*-binding proteins (spots 851 and 964) were more abundant in response to Cd treatment and one protein (spot 964) was more abundant in response to Zn treatment compared with the control. Two proteins involved in PSII assembly and stabilization were more abundant in response to both Cd and Zn (spots 712 and 1072) treatment compared with the control. The 10 kDa protein involved in PSII structure (spot 1179) was less abundant in response to Zn treatment, one protein involved in the transfer of electrons was more abundant in response to both Cd and Zn treatment (spot 986) compared with the control.

In relation to carbohydrate metabolism, 2 Rubisco activases (spots 412 and 418) were more abundant in response to Cd treatment and 7 Rubisco activases (spots 342, 408, 412, 418, 426, 447 and 454) were more abundant in response to Zn treatment compared with the control. Looking at the gel image (Fig. 4), the Rubisco large subunit appeared fragmented (spots 318 to 1143), taking into account the molecular weight where the Rubisco large subunit is expected (spots 212 to 300). Interestingly, three proteins corresponding to the Rubisco large subunit were more abundant in response to Cd treatment (spots 213, 218 and 219) and six were more abundant in response to Zn treatment (spots 212, 213, 218, 219, 233 and 296) compared with the control, while 21 polypeptides corresponding to the fragments of the Rubisco large subunit were less abundant in response to Cd treatment and 22 were less abundant in response to Zn treatment compared with the control. The chloroplast sedoheptulose-1,7-biphosphatase involved in the Calvin cycle (spot 486) was more abundant in response to both Cd and Zn treatment, two phosphoglycerate kinases were more abundant in response to Zn treatment only (spots 361 and 373), and one glycoside hydrolase (spot 610) was more abundant in response to Zn treatment compared with the control. Regulation of proteins related to the glycolysis pathway was affected only in response to Zn treatment; one phosphoglycerate kinase (spot 436), a fructose–bisphosphate aldolase (spot 472) and a glyceraldehyde-3-phosphate dehydrogenase subunit 1 (spot 507) were more abundant in leaves of Zn-treated plants than in leaves of the controls.

Amino acid and protein biosynthesis function were little affected by metal treatments; a protein involved in methionine synthesis was more abundant in response to Zn treatment compared with the control (spot 65).

All the proteins involved in energy and metabolism function, which regulation was affected by treatments, were more abundant in leaves of treated plants compared with the controls. Notably, four proteins which are related to the subunit of ATP-synthase were more abundant in response to both Cd and Zn treatment (spots 225, 226, 236 and 249); two others were also more abundant in response to Zn treatment (spots 250 and 470).

Of the three proteins involved in antioxidant defence and detoxification, one quinone oxidoreductase-like protein was more abundant in response to Cd treatment (spot 529) and two quinone oxidoreductase-like proteins and a FeSOD were more abundant in response to Zn treatment (spots 529, 530 and 808) compared with the control.

Plant water status and related photosynthesis parameters

The leaf area of elongating leaves increased faster for the control and Zn-treated plants than for Cd-treated ones (Fig. 5a; $P = 0.0155$ and $P = 0.0021$ after 14 and 28 d, respectively). As a result, the leaf area was significantly lower for Cd-treated plants than for controls after both 14 and 28 d. Directly related to this leaf expansion, Cd treatment significantly increased SD after 28 d of treatment ($P = 0.0280$; Fig. 5b), while it had no impact on the SI nor on the total stomata number on the leaf abaxial side (detailed data not shown).

The WC in elongating leaves significantly decreased after 28 d in response to Cd treatment ($P = 0.0392$) and already after 14 d in response to Zn treatment ($P = 0.0005$) compared with the control (Fig. 5c). Leaf Ψw was not significantly affected during the experiment (results not shown). Leaf Ψs_{cor} significantly decreased in response to 28 d of Cd treatment compared with the control ($P < 0.0001$; Fig. 3)

Table 3. Cadmium- or Zn-induced differentially expressed proteins in *Zygophyllum fabago* leaves identified by MALDI-TOF analysis after 28 d of treatment with 10 μM Cd or 50 μM Zn

Spot number[a]	Homologous protein[b]	Fold change Cd/control[c]	Fold change Zn/control[c]	Fold change Cd/Zn[c]
Photosynthetic apparatus-related proteins				
851	Chlorophyll *a*/*b* binding protein, putative	2.42	2.00	1.21
964	Chlorophyll *a*/*b* binding protein	1.77	1.89	−1.07
1179	Photosystem II 10 kDa polypeptide	−1.07	−1.53	1.43
1197	Photosystem I reaction centre subunit N, chloroplast precursor, putative	1.66	−1.13	1.87
986	Cytochrome b6-f complex iron-sulphur subunit, chloroplastic	2.00	2.11	−1.05
712	Oxygen-evolving enhancer protein 1, chloroplastic	2.86	2.42	1.18
888	Oxygen-evolving enhancer protein 2, chloroplastic	−1.19	1.78	−2.12
1072	Oxygen-evolving enhancer protein 3 precursor	1.84	1.75	1.05
Protein biosynthesis				
65	Vitamin-b12 independent methionine synthase, 5-methyltetrahydropteroyltriglutamate-homocysteine	1.20	2.05	−1.70
105	Heat shock 70 kDa protein, mitochondrial; precursor	−1.02	1.50	−1.53
Energy and metabolism				
225	ATP synthase CF1 alpha subunit	2.39	3.04	−1.27
226	ATP synthase CF1 alpha subunit	2.20	3.76	−1.71
236	ATP synthase subunit B	3.34	2.74	−1.22
249	ATP synthase beta subunit	2.15	2.55	−1.19
250	ATP synthase beta subunit	1.78	2.78	−1.56
325	Sulphate adenylyltransferase, putative	1.50	1.53	−1.02
470	ATP synthase gamma chain 2, chloroplast, putative	1.31	1.80	−1.38
509	Putative RNA binding protein	1.35	1.68	−1.24
477	Putative mRNA binding protein precursor	1.34	1.93	−1.43
Carbohydrate metabolism				
342	Rubisco activase 1, putative	1.33	2.32	−1.74
408	Rubisco activase 1	1.48	2.49	−1.69
412	Rubisco activase	1.79	2.00	−1.12
418	Rubisco activase 1	1.91	1.97	−1.03
426	Rubisco activase 1	1.62	1.57	1.03
447	Rubisco activase 1	1.76	1.89	−1.07
454	Rubisco activase 1	1.11	1.52	−1.37
212	Rubisco large subunit	2.29	2.49	−1.09
213	Rubisco large subunit	1.94	2.49	−1.28
218	Rubisco large subunit	3.46	3.23	1.07
219	Rubisco large subunit	2.49	2.66	−1.07
233	Rubisco large subunit	2.07	3.52	−1.70
289	Rubisco large subunit	1.94	3.48	−1.79
296	Rubisco large subunit	1.76	3.47	−1.97
300	Rubisco large subunit	−1.02	1.64	−1.67
318	Rubisco large subunit degraded	−1.56	−1.68	1.08
322	Rubisco large subunit degraded	−1.92	−2.42	1.26
332	Rubisco large subunit degraded	−3.75	−5.07	1.35
341	Rubisco large subunit degraded	−1.76	−2.04	1.16
355	Rubisco large subunit degraded	−2.15	−2.61	1.22
394	Rubisco large subunit degraded	−1.60	−2.20	1.37
484	Rubisco degraded	−4.43	−6.24	1.41
485	Rubisco large subunit degraded	−4.48	−7.77	1.73

505	Rubisco large subunit degraded	−5.28	−7.66	1.45
508	Rubisco large subunit degraded	−5.63	−8.54	1.52
511	Rubisco large subunit degraded	−2.45	−3.21	1.31
614	Rubisco large subunit degraded	−6.66	−13.99	2.10
618	Rubisco large subunit degraded	−8.71	−20.07	2.31
640	Rubisco large subunit degraded	−7.87	−14.80	1.88
642	Rubisco large subunit degraded	−2.95	−3.06	1.04
662	Rubisco large subunit degraded	−2.91	−5.21	1.79
666	Rubisco large subunit degraded	−6.03	−8.28	1.37
725	Rubisco large subunit degraded	−2.62	−2.71	1.03
734	Rubisco large subunit degraded	−4.34	−7.30	1.68
845	Rubisco large subunit degraded	−2.52	−2.65	1.05
896	Rubisco large subunit degraded	−2.40	−6.34	2.64
942	Rubisco large subunit degraded	−2.90	−5.27	1.82
1143	Rubisco large subunit degraded	−3.81	−2.40	−1.59
361	Phosphoglycerate kinase, chloroplastic; precursor	1.55	2.70	−1.74
373	Phosphoglycerate kinase, chloroplastic; precursor	1.74	1.54	1.13
486	Chloroplast sedoheptulose-1,7-bisphosphatase	1.60	1.64	−1.02
610	Lichenase precursor, putative	1.48	1.70	−1.15
Glycolysis				
436	Phosphoglycerate kinase, cytosolic	1.22	2.06	−1.69
472	Fructose-bisphosphate aldolase, putative	1.65	2.90	−1.75
507	Glyceraldehyde-3-phosphate dehydrogenase subunit 1 (GapC)	1.52	2.45	−1.61
Oxido-reductase activity (oxidative stress response)				
529	Quinone oxidoreductase-like protein	1.51	1.94	-1.28
530	Quinone oxidoreductase-like protein	1.38	2.38	-1.72
808	FeSOD	1.48	1.93	-1.31

[a]Numbering according to Fig. 4; for detailed identification data, see Supporting Information Table S1.
[b]NCBI protein database; either the name of the highest scoring protein is given or in the case a protein was identified based on the EST database, the EST sequence was blasted and the protein with the highest, significant homology given.
[c]Average ratios of the protein abundance (stressed/control). For those time points that both the ratio in relative abundance is below −1.5 or above 1.5 and the *t*-test score $P < 0.05$, the value of the ratio is shaded: black indicates up-regulation; grey indicates down-regulation.

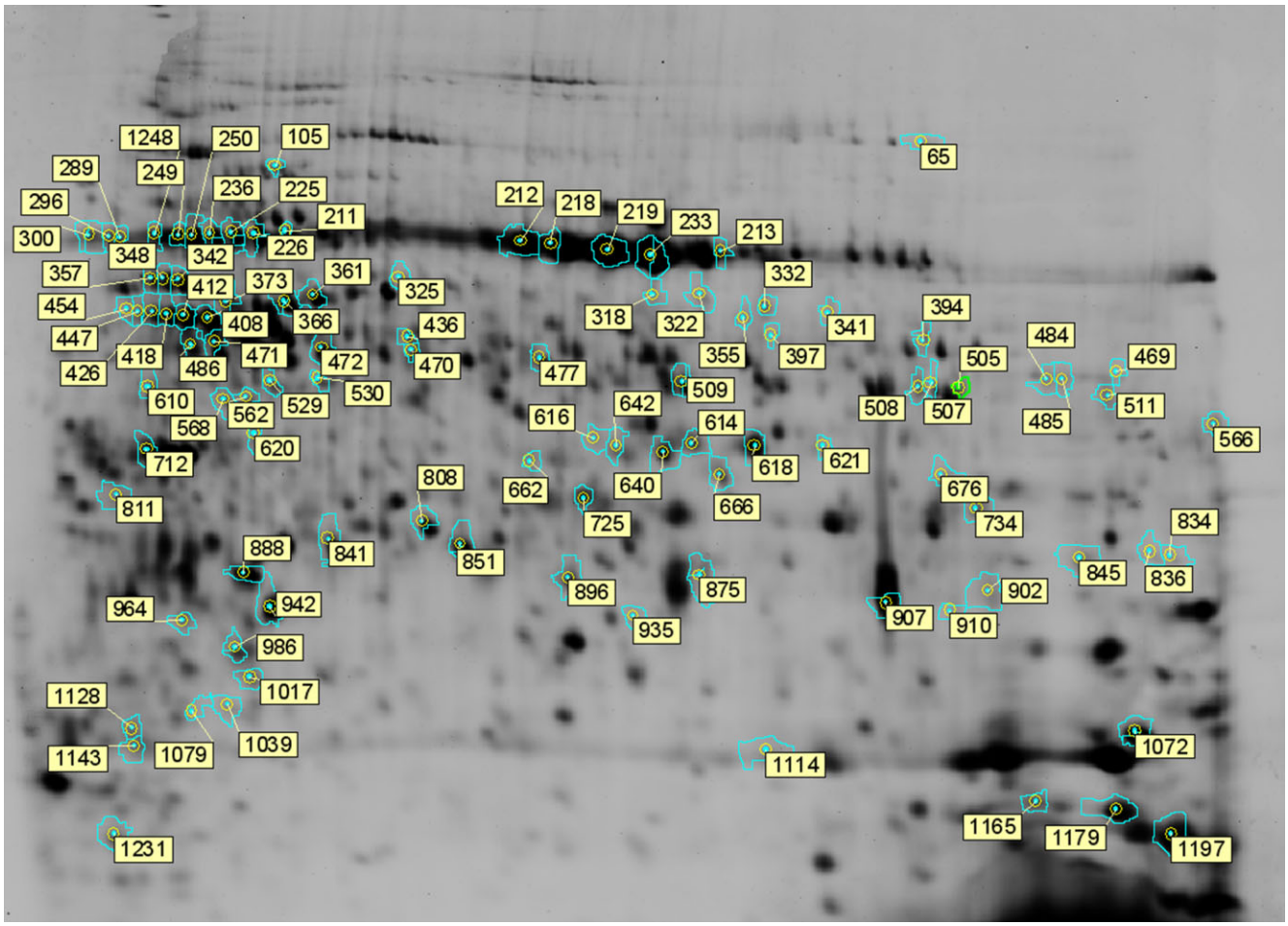

Figure 4. A representative 2D-electrophoresis gel of *Zygophyllum fabago* leaf samples after 2 weeks of treatment. Indicated on the image are the spots significantly affected during the experiment. The spot numbering corresponds to the numbering used in Table 3 and in Supporting Information Table S1.

and already after 14 d of Zn treatment compared with the control ($P = 0.0033$), thereafter remaining stable during the experiment (Fig. 5d).

Stomatal conductance (g_l) of elongating leaves significantly decreased in response to Zn excess compared with the control and Cd after 14 d of treatment (Fig. 6a). This difference disappeared with time since leaf g_l of control plants significantly decreased with time ($P = 0.0016$; Fig. 6a). The instantaneous CO_2 assimilation rate (A) remained unaffected during the whole experiment (Fig. 6b). The leaf g_l decrease of Zn-treated plants was concomitant with a slight decrease of leaf E and a slight increase of A/E ratio. These parameters were only significantly different from those of Cd-treated plants, which presented an inverse trend (Fig. 6c,d). These differences disappeared with time. When considering E of the whole leaf area, this parameter significantly decreased already after 14 d of Cd treatment (results not shown; $P = 0.0180$). After 28 d of treatment, $\Delta^{13}C$ was significantly lower in elongating leaves of plants exposed to Cd or Zn ($P < 0.0001$; Fig. 6e).

Cd or Zn treatment had no effect on Chl *a* and carotenoids concentration in elongating leaves, while Zn significantly increased Chl *b* concentration after 14 d of treatment ($P = 0.0474$; Table 4). This difference disappeared with time. Despite this increase, no significant difference was recorded for Chl *a*/*b* ratio (Table 4). Cd or Zn treatment had no impact on F_0 of elongating leaves, while a significant decrease of F_v/F_m occurred after 14 d of Zn treatment to the end of the experiment, and after 28 d of Cd treatment ($P = 0.0262$ and $P = 0.0029$ after 14 and 28 d, respectively; Table 4).

Metabolite analysis

Cd K-edge and Zn K-edge EXAFS spectra were measured in the shoots of Zn- and Cd-treated plants as well as in some Zn and Cd model compounds (not shown for Zn, for Cd refer to Koren *et al*. 2013). Since no chemical pretreatment were performed during sample preparation, the metal–ligand environment was not altered and did not result in the formation of some complexes that were absent *in vivo*. To circumvent the unwanted appearance of metal complexes as a result of extraction and/or separation procedures, X-ray absorption spectroscopy is ideal as it probes the coordination geometry of metals in plants with minimal tissue disturbance.

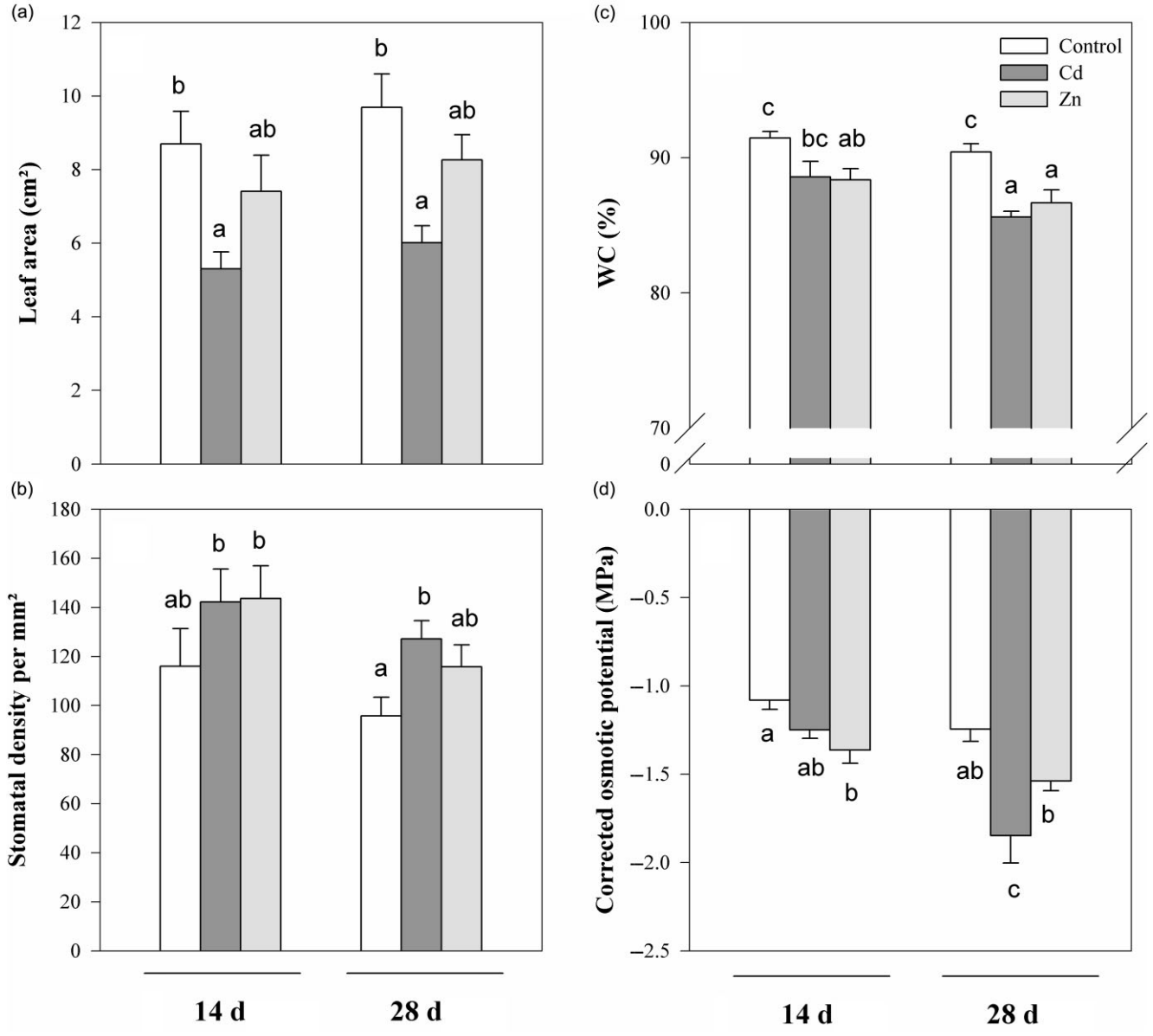

Figure 5. Leaf area (a), stomatal density (b), water content (WC) (c) and corrected osmotic potential (d) in leaves of *Zygophyllum fabago* in the absence (control) or in the presence of 10 μM Cd or 50 μM Zn after 14 and 28 d of treatment. Values are based on the means of six replicates, vertical bars are SE. For each of the parameters, histograms showing the same letter are not significantly different at $P < 0.05$ level.

Fourier transform magnitudes of Cd K-edge and Zn K-edge EXAFS spectra of leaves already indicated differences in the contribution of the nearest Cd or Zn atoms between the treatments (Fig. 7). The quantitative structural information of the local Cd and Zn neighbourhood (type and average number of neighbour atoms, their distance from Cd or Zn atom, and Debye–Waller factor of neighbouring shells [measuring the thermal and structural disorder in the shells]) was obtained by a quantitative EXAFS analysis, already described in details by Vogel-Mikuš *et al*. (2010a), in which the model EXAFS function was fitted to the measured EXAFS spectra. The best-fit parameters for all the samples are presented in Fig. 7 and represent an average Cd and Zn environment in the investigated organ. They indicate an average first shell coordination of S/O/N in all samples for both atoms. A higher number of S (61%) than O/N (39%) ligands was found for Cd in the shoots. The opposite was observed for Zn coordination with a lower number of S (39%) ligands than O/N (61%) ligands found in the shoots. The Debye–Waller factors in the first coordination shell remained lower than 0.010, indicating a low static disorder, hence the presence of predominant Zn and Cd complexes.

For the assay of acid-soluble thiols, the recoveries of the internal standard GSH added to the leaf material were more than 98%, indicating that loss and oxidation of thiol compounds did not occur in the extracts. Cadmium treatment induced a highly significant increase of acid-soluble thiol concentration compared with control ones after 14 d to the end

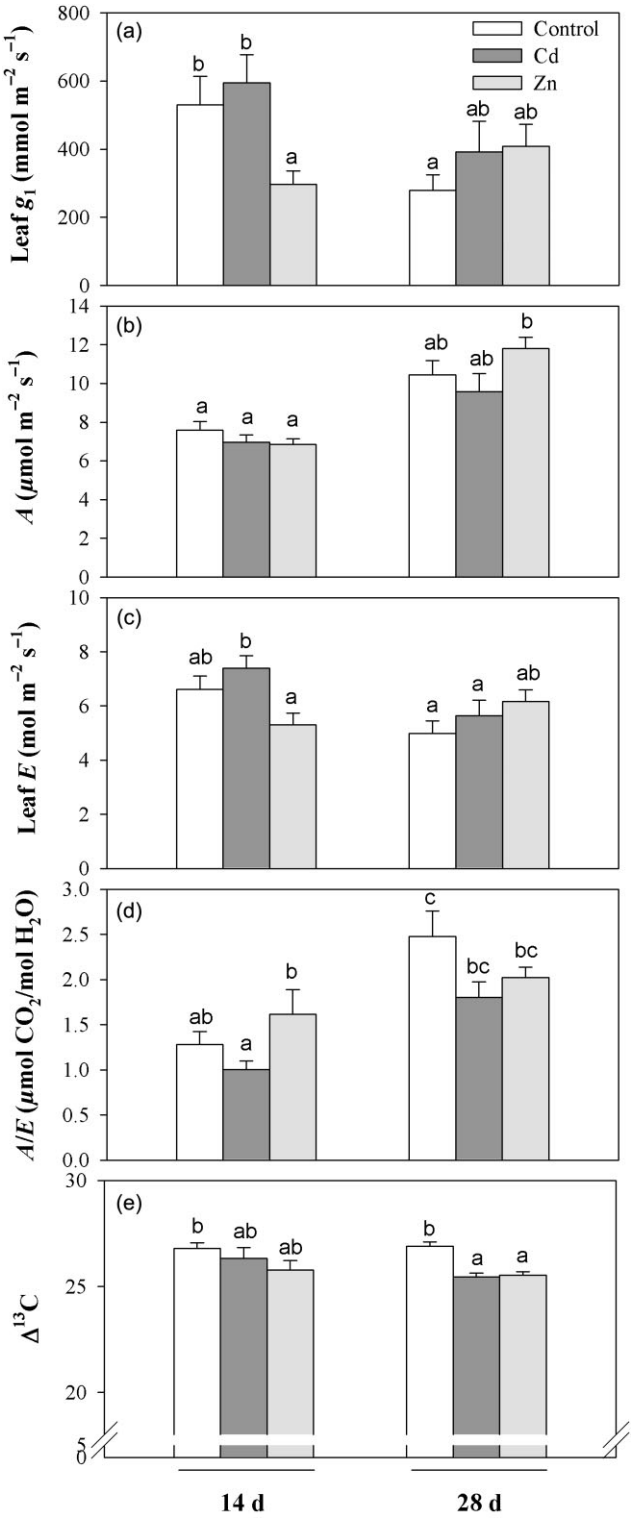

Figure 6. Leaf stomatal conductance (a), CO_2 assimilation rate (b), transpiration rate (c), CO_2 assimilation rate/transpiration rate ratio (d) and carbon isotope discrimination (e) in leaves of *Zygophyllum fabago* in the absence (control) or in the presence of 10 μM Cd or 50 μM Zn after 14 and 28 d of treatment. Values are based on the mean of six replicates, vertical bars are SE. For each of the parameters, histograms showing the same letter are not significantly different at $P < 0.05$ level.

of the experiment ($P < 0.0001$; Fig. 8a), while no significant change in the acid-soluble thiol concentration was observed in response to Zn compared with the controls whatever the duration of the treatment. However, in response to both Cd and Zn treatment, a decrease in the acid-soluble thiol concentration was observed after 28 d of treatment compared with 14 d of treatment ($P = 0.0170$ and $P = 0.0388$, respectively).

The proline concentration significantly and progressively increased in elongating leaves of Cd-treated plants compared with control ones after already 14 d until the end of the experiment ($P = 0.0460$). It also significantly increased in elongating leaves of Zn-treated plants after 28 d, but remained significantly lower than in Cd-treated plants ($P = 0.0001$; Fig. 8b).

Both Cd and Zn treatment progressively and significantly increased the total soluble sugar concentration in elongating leaves compared with control ones after already 14 d of treatment ($P = 0.0010$; Fig. 8c).

DISCUSSION

The present study followed the physiological and metabolic status of *Z. fabago* leaves, which were elongating at the beginning of Cd and Zn treatments and fully expended at the end of the experiment. Although Cd and Zn have been shown to share numerous physicochemical properties and are commonly found simultaneously in contaminated soils, our work highlighted the different strategies that *Z. fabago* developed in response to each considered element.

Zygophyllum fabago displays ion-specific physiological responses to overcome Cd or Zn toxicities in leaves

In response to a moderate Cd treatment, the Cd concentration rapidly increased in leaves (Fig. 1a) to reach a maximum value within less than a week, as previously shown by Lefèvre *et al.* (2009). Despite this rapid Cd accumulation, the decrease in leaf WC and osmotic Ψs, already reported for this species (Lefèvre *et al.* 2005, 2009, 2010a), occurred after only 28 d in response to Cd treatment. Cadmium induced a reduction of the leaf expansion compared with the controls and a resulting increase in stomatal density (Fig. 5). This reduction of leaf area in response to Cd without any modification of leaf g_l, implies the limitation of whole leaf transpiration, even if stomatal density increased. It may be considered as a strategy to maintain cell turgor over a short period of treatment in relation to a putative decrease in cell wall extensibility (Aidid & Okamoto 1993; Wehr *et al.* 2004). A progressive increase in the concentration of proline and soluble sugars pointed out the synthesis of osmo-protecting compounds as one of the mechanisms set up on Cd long-term treatment (Fig. 8). A different pattern was observed in response to Zn treatment since Zn accumulated regularly in leaves over the whole experiment (Fig. 1b). This difference in the regulation of Cd and Zn absorption and translocation by *Z. fabago* was already evidenced by Lefèvre *et al.* (2010a). Despite a

Table 4. Effect of 10 μM Cd or 50 μM Zn treatment on the concentration of pigments, Chl *a*/*b* ratio and chlorophyll fluorescence parameters of *Zygophyllum fabago* after 14 and 28 d of treatments

	Treatments	Chl *a* (μg g^{-1} FM)	Chl *b* (μg g^{-1} FM)	Carotenoids (μg g^{-1} FM)	Chl *a*/*b*	F_0	F_v/F_m
14 d	Control	809 ± 34a	251 ± 9a	196 ± 9a	3.230 ± 0.047a	0.272 ± 0.005a	0.841 ± 0.004b
	Cd	815 ± 28a	247 ± 8a	213 ± 8a	3.294 ± 0.034a	0.269 ± 0.004a	0.836 ± 0.003ab
	Zn	913 ± 36a	285 ± 14b	224 ± 8a	3.211 ± 0.056a	0.280 ± 0.008a	0.824 ± 0.006a
28 d	Control	813 ± 45a	252 ± 14a	186 ± 11a	3.228 ± 0.022a	0.262 ± 0.003a	0.845 ± 0.002b
	Cd	830 ± 42a	257 ± 12ab	217 ± 6a	3.232 ± 0.029a	0.274 ± 0.006a	0.829 ± 0.003a
	Zn	868 ± 36a	277 ± 13ab	202 ± 8a	3.140 ± 0.050a	0.284 ± 0.009a	0.825 ± 0.006a

Values are means ± SE, $n = 6$. Values in the same column showing the same letter are not significantly different at $P < 0.05$ level.

progressive Zn accumulation in leaves, some physiological modifications were observed after already 14 d of Zn treatment. While no modification in leaf expansion nor stomatal density was observed in response to Zn treatment unlike Cd-treated ones, a decrease in WC was observed after 14 d of Zn treatment associated with a transient decrease of leaf osmotic Ψs and g_l, associated with a rapid increase in soluble sugars, which may contribute to the observed osmotic adjustment (Figs 5, 6 & 8). This decrease in leaf Ψs and g_l may partly counteract the water stress during the first 14 d of Zn treatment, while some other mechanisms were probably set up on long-term treatment, as discussed thereafter. A significant reduction in leaf transpiration was observed after 14 d of Zn treatment compared with Cd treatment, highlighting specific mechanisms drawn up in response to different ions.

Zygophyllum fabago is able to maintain net photosynthesis over the whole experiment whatever the treatment

A decrease in $\Delta^{13}C$ in the *Z. fabago* C3 plant after 28 d of Cd or Zn treatment supported the idea of a decrease in leaf CO_2 diffusion in response to both treatments since variation of $\Delta^{13}C$ has been shown to be strongly dependent on the intercellular CO_2 pressure (*Ci*) (Farquhar *et al*. 1989). Several studies indeed reported an effect of Cd on stomatal resistance related to an interference with Ca signalling in guard cells (Ghelis *et al*. 2000; Perfus-Barbeoch *et al*. 2002). In our experiment, such stomatal resistance increased only in response to 14 d of Zn application and may not explain $\Delta^{13}C$ decrease in response to Cd treatment. However, stomatal resistance is not the only parameter accounting for lower CO_2 concentration in the leaf tissues. The less-well-known diffusion pathway in the mesophyll, from the substomatal cavities to the sites of carboxylation, is estimated to account for around 40% of the decrease in CO_2 concentration between the atmosphere and sites of carboxylation, as reviewed by Warren (2008) and Sharkey (2012). Whatever this limitation in CO_2 diffusion, no decrease in net photosynthesis was recorded over the whole experiment and leaves from Zn-treated plants of *Z. fabago* exhibited higher instantaneous water use efficiency after 14 d of stress as shown by the higher *A*/*E* ratio (Fig. 6). An increase in Rubisco, in some proteins involved in the Calvin–Benson cycle and in K concentration in palisade mesophyll in *Z. fabago* leaves, described in more details hereafter, may counteract the CO_2 limitation through a higher efficiency in photosynthetic CO_2 fixation.

While photosynthetic parameters remained unaffected as a result of 14 d of Cd treatment, a decrease in the F_v/F_m ratio was observed in response to Zn treatment, indicating a decrease in the PSII efficiency, probably partly associated with the decrease in the concentration of the 10 kDa polypeptide involved in PSII assembly (Table 3), a protein that provides a binding site for the extrinsic oxygen-evolving complex protein PsbP to the thylakoid membrane. An increase in the abundance of PsbP (spot 888), as well as some other proteins involved in the LHCII structure, the electron transfer chain and oxygen-evolving complex, may occur as a compensation of a decrease in the quality of the PSII (Table 3).

Proteome analysis also revealed that, after 14 d, both treatments induced modifications in the abundance of proteins mainly involved in the photosynthetic apparatus, carbohydrate and C-metabolism (Table 3). It is important to notice that nearly all the identified proteins increased in abundance in response to ion toxicity. Among these proteins, it is interesting to notice an increase in the abundance of Rubisco and in proteins associated with the Calvin–Benson cycle in response to Cd and Zn treatment, and a decrease in the level of degradation of the Rubisco large subunit. This uncommon response may be related to a preservation of the photosynthetic activity, at a time when the CO_2 diffusion is altered. The considered *Z. fabago* material is originating from a metallicolous site (Lefèvre *et al*. 2010a) and it may have set up these mechanisms to survive in a drastic environment. Van Assche & Clijsters (1990) proposed that a modification in Rubisco activity, resulting in a decrease in carboxylation/oxygenation ratio, may be induced by toxic metals, and an up-regulation in the synthesis of this protein may thus counteract a lower activity. Rubisco catabolism is an important process in leaf maturation and senescence, and notably contributes to N remobilization (Feller *et al*. 2008). A fragmentation of the Rubisco large subunit has been evidenced in response to various abiotic stresses (Pietrini *et al*. 2003; Nakano *et al*. 2006; Feller *et al*. 2008). Some results suggested that the Rubisco large subunit may be non-enzymatically cleaved by oxygen radicals, and that the effects of various

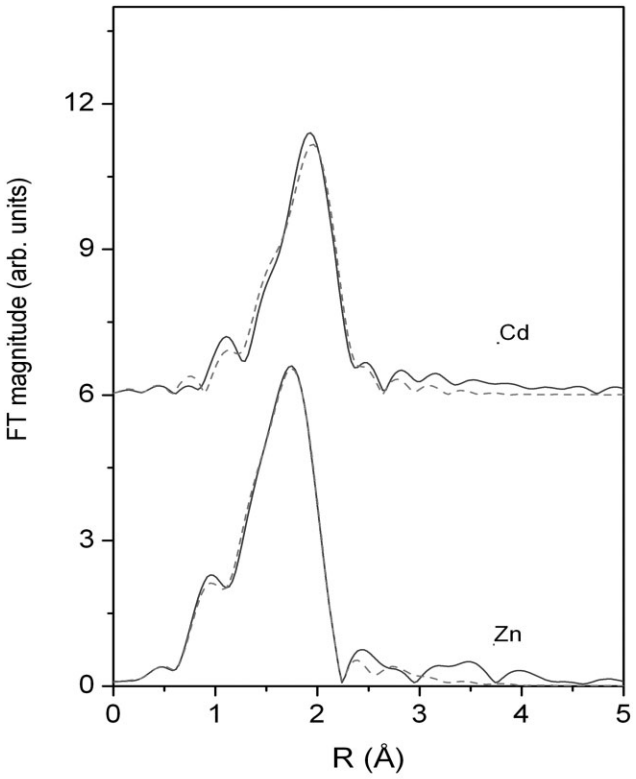

Cd treatment

Cd neighbour	*N*	R (Å)	σ^2 (Å^2)	% *N*
O	2.2(5)	2.19(1)	0.009(3)	**39%**
S	3.4(5)	2.48(1)	0.007(3)	**61%**

Zn treatment

Zn neighbour	*N*	R (Å)	σ^2 (Å^2)	% *N*
O	3.5(7)	2.02(1)	0.0010(4)	**61%**
S	2.2(5)	2.29(1)	0.008(2)	**39%**

Figure 7. Figure above represents the Fourier transform magnitudes of EXAFS spectra (solid line), together with the best-fit EXAFS model (dashed line) calculated in the *k* range of 3.0–13 Å^{-1} and *R* range from 1.0 to 3.0 Å for Cd in response to 10 μM Cd treatment and calculated in the *k* range of 3.0–12 Å^{-1} and *R* range from 1.0 to 2.7 Å for Zn in response to 50 μM Zn treatment. Table below represents parameters of the nearest coordination shells around the Cd or Zn atoms in leaves of *Zygophyllum fabago* treated with 10 μM Cd or 50 μM Zn for 1 month. *N*, number of nearest neighbour atoms; R, distance; σ^2, Debye–Waller factor. The uncertainty of the last digit is given in parentheses.

ROS scavengers can counteract this cleavage (Ishida *et al.* 1999; Nakano *et al.* 2006). In our case, maintaining Rubisco abundance through a decrease in its degradation may be a mechanism of energy cost limitation in C-metabolic pathways. Associated to an up-regulation of some proteins involved in the photosynthetic apparatus and C-metabolism (Table 3), it resulted in an increase in the sugar concentration, already observed after 14 d both in response to Cd and Zn treatments (Fig. 8), and to an increase in the energy production in response to Zn treatment suggested by the increase in abundance of some enzymes involved in the

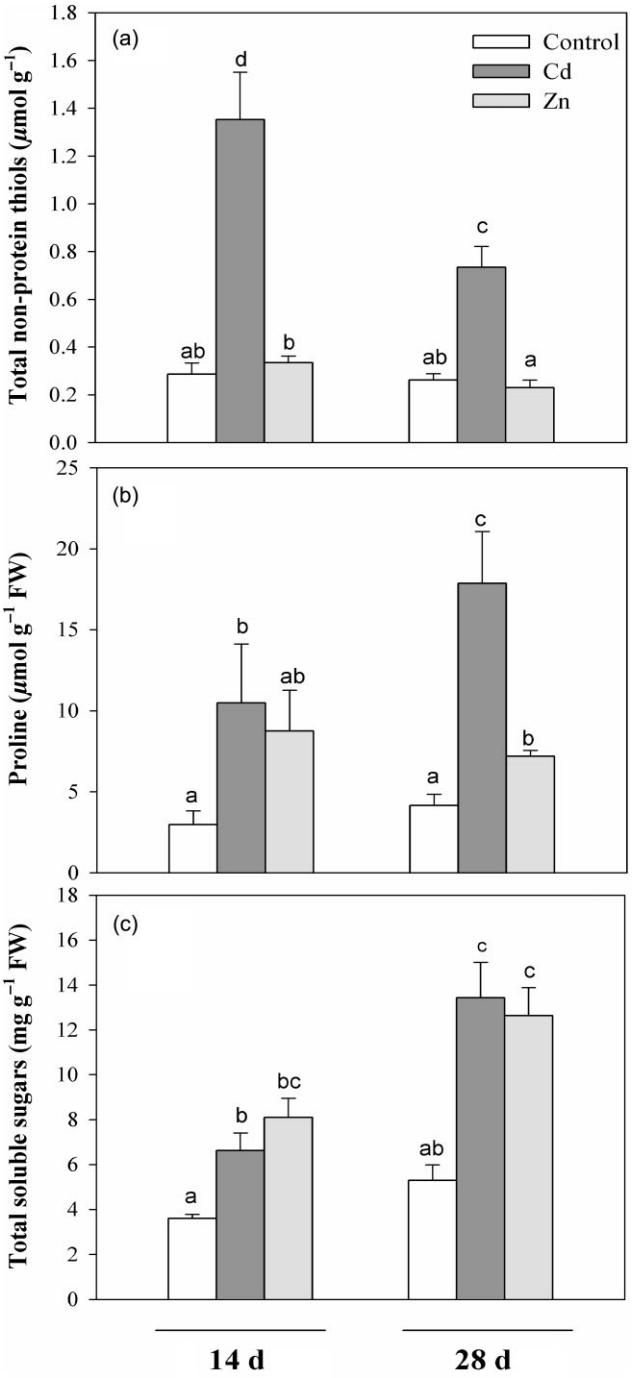

Figure 8. Total non-protein thiols (a), proline (b) and total soluble sugars (c) concentrations in leaves of *Zygophyllum fabago* in the absence (control) or in the presence of 10 μM Cd or 50 μM Zn after 14 and 28 d of treatment. Values are based on the mean of six replicates, vertical bars are SE. For each of the parameters, histograms showing the same letter are not significantly different at $P < 0.05$ level.

glycolysis pathways. At this stage of development, *Z. fabago* may favour sugar synthesis rather than sugar mobilization through starch conversion as observed by Kieffer *et al*. (2008) in poplar exposed to Cd treatment.

As already mentioned, while an increase in the abundance of proteins involved in glycolysis, pentose phosphate pathway, and oxidative stress defence is usually recorded in response to Cd and Zn treatment (Yuan *et al*. 2009; Villiers *et al*. 2011), such an up-regulation of proteins involved in C-metabolism as observed in *Z. fabago* leaves is rarely recorded in other species, even at short-term metal exposure and/or mild stress. To the best of our knowledge, such an increase in proteins involved in photosynthesis was only reported in a high Cd-accumulating soybean cultivar and in *Arabidopsis thaliana* in response to short-term exposure to 10 and 100 μM Cd, respectively (Semane *et al*. 2010; Hossain *et al*. 2012). Moreover, proteins involved in energy function were more abundant in *Z. fabago* in response to Cd or Zn treatment compared with control, while a decrease in their level is usually observed in response to these treatments (Fukao *et al*. 2011; Villiers *et al*. 2011). These data reinforce our hypothesis that the present *Z. fabago* metallicolous plants are somewhat able to behave as a heavy metal-resistant plant species (Lefèvre *et al*. 2005). Altogether, such an increase in proteins indicated the importance of photosynthesis and energy production in plant survival to ion toxicity, as already demonstrated by Sarry *et al*. (2006) in Cd-exposed *A. thaliana* cell cultures.

With regard to the increase in abundance of a large number of proteins involved in photosynthetic apparatus and C-metabolism, a surprisingly low number of proteins involved in oxidative stress response was identified, while an oxidative stress has already been evidenced after 14 d of Cd treatment (Lefèvre *et al*. 2009). After 28 d of Cd treatment, proteome analysis of *Z. fabago* revealed that the photosynthetic apparatus-related proteins were affected, but we observed an increase in the number of up-regulated stress-defence proteins (catalase, endo-β-1,3-glucanase, chitinase; unpublished results), underlying an evolution in the strategy of plant response with the duration of the exposure. However, the number of these stress-defence proteins remained limited in comparison with other non-hyperaccumulating species (Hossain *et al*. 2012). A previous study performed on proliferating callus culture of *Atriplex halimus* indicated that the most resistant cell lines to Cd displayed a high constitutive superoxide dismutase activity and an efficient Cd-induced increase in glutathione reductase and ascorbate peroxidase activity (Lefèvre *et al*. 2010b). These results suggested that the antioxidant response is not necessarily related to any transcriptional or translational regulation, but may be related to a stimulation of enzyme activity.

Zygophyllum fabago limits Cd and Zn translocation to photosynthetically active tissues and reallocates other essential elements

The preservation of photosynthetic activity previously mentioned over at least the first 14 d in response to both Cd and Zn treatments may be related to the toxic ion distribution in tissues. Indeed, micro-PIXE analysis revealed an increase of Zn concentration preferentially in the vascular bundle and spongy mesophyll (Table 1). LA-ICP-MS mapping suggested some hot spots of Cd accumulation near the vascular bundle (Fig. 3). These results are in accordance with a protection of the photosynthetic activity through a limitation of toxic elements in the palisade mesophyll. Recent results obtained by Cestone *et al*. (2012) on spatial distribution of Cu in *Brassica carinata* indicate, through the use of H^+-ATPase inhibitor vanadate, some energy-dependent processes involved in Cu accumulation within the vein parenchyma cells. Such active mechanisms may be considered also in the case of Cd and Zn accumulation in leaf tissues of *Z. fabago*.

Although it accumulated to lower levels than Zn, Cd had a drastic influence on element redistribution between tissues. It is probably related to the fact that Cd enters plant cells via uptake systems for essential cations. However, a number of similarities were reported in essential ion redistribution. Competition between divalent cations may explain the decrease in Ca concentration observed in palisade and spongy mesophyll in response to both Cd and Zn treatments. An increase of the Ca concentration in phloem suggests the remobilization of this element to other sink tissues. Another important feature is the increase of the K concentration in palisade mesophyll in response to both Cd and Zn treatments. Potassium is the dominant counterion to the light-induced H^+ flux across the thylakoid membranes and for the establishment of the transmembrane pH gradient necessary for the synthesis of ATP (Marschner 1995). Its protective role in the maintenance of photosynthetic CO_2 fixation has already been reported in response to abiotic stress (Cakmak 2005) and appeared to be another important mechanism of protection against ion toxicity in *Z. fabago* leaves. Since a water stress occurred after 28 d of treatment, K may also be involved in the osmotic adjustment previously mentioned. This element has also been reported to counteract metal toxicity by improving activity of antioxidant enzymes and solutes (Siddiqui *et al*. 2012).

Ion-specific ligands are involved in Cd or Zn complexation in *Z. fabago* leaves

Since no competition was recorded between divalent cations and S assimilation, a decrease of S in palisade and spongy mesophyll is probably linked to a remobilization of this element to other tissues. Indeed, EXAFS results indicated S as the first neighbour atom for more than 60% of the Cd (Fig. 7), suggesting that Cd is mainly bound to S-containing compounds. Considering the increase in S concentration in phloem and sclerenchyma tissues, these results tend to confirm a higher Cd allocation suspected in the area of the vascular bundle. The large amount of Cd bound to S compounds is in accordance with the large increase of non-protein thiols we observed in response to Cd (Fig. 8). Cadmium indeed has a high affinity for thiol-containing compounds, such as glutathione, phytochelatins and the sulphur-containing amino acid (Gallego *et al*. 2012; Koren *et al*. 2013).

Less than 40% of Cd is bound to O as a first neighbour atom. O ligands are rather weak and less specific. They can either be hydroxyl or carboxyl groups of organic acids, such as citrate or malate (Vogel-Mikuš *et al*. 2010a; Koren *et al*. 2013). The cell wall mainly contains O ligands like carboxyl and hydroxyl groups, so it might not be distinguished properly from other O ligands. Generally, EXAFS analysis cannot discriminate between N and O ligation. Since sclerenchyma appeared to be a preferential site for Cd accumulation, this element may be bound to lignin. Indeed, lignin displays ligand properties given by hundreds of interlink phenolic ring subunits of lignin, most of which being phenylpropene-like structures with various methoxyl ($-OCH_3$), hydroxyl (–OH), benzyl alcohol and aldehyde functional groups.

We observed the reverse trend for Zn with the first neighbour atom corresponding to O for more than 60% and to S for less than 40%. Our results indicate that the Zn concentration increased both in apoplasm and cytoplasm (Table 2). Cell wall binding can therefore not solely explain this complexation. The Zn–O ligand distances of 2.02 Å fit well with distances reported for model compounds and a protein crystal structure (Zn–His, approximately 2.00; and Zn–O, 1.95–2.14; Harding 2001). The literature often reports organic compounds and amino acids as ligands, especially histidine and cysteine (Terzano *et al*. 2008; Zeng *et al*. 2011). Through micro-XANES analysis, Terzano *et al*. (2008) reported that Zn was for ~50% in the form of P precipitates, and the other 50% complexed by cysteine and histidine residues. Our results did not support a complexation to cysteine in *Z. fabago* since no increase in non-protein thiol compounds occurred during the whole Zn treatment, nor to P, but an accumulation of histidine may be hypothesized. The non-proteinogenic amino acid niotianamine (NA) displays an important role in Zn homeostasis in plants (Deinlein *et al*. 2012; Haydon *et al*. 2012; Schuler *et al*. 2012). Considering the high level of Zn concentration in both xylem and phloem and the distance of its nearest neighbour atom (Fig. 7; Zn–NA 2.093 ± 0.003 Å; Trampczynska *et al*. 2010), NA may be considered as a Zn ligand. Indeed, Trampczynska *et al*. (2010) recorded a high Zn affinity with NA, displaying a complexation rather rigid than with organic acid ligands. However, these authors also demonstrated that the importance of NA contribution to Zn ligation is still controversial in hyperaccumulators. In this way, malate or citrate also appeared to be good candidates for Zn ligation in leaves (Zn–malate 2.01 ± 0.010 Å, Zn–citrate 2.03 ± 0.010 Å) (Trampczynska *et al*. 2010; Sarret *et al*. 2002).

CONCLUSIONS

Through an integrated study of ion histological distribution, plant physiological status, proteomic and metabolite analyses, this study evidenced the importance of ion localization at the tissue and cell level in the mechanism of plant response to heavy metal accumulation. Though *Z. fabago* was able to induce a protection of the photosynthetically active tissues and maintenance of cell turgor in leaves through the reallocation of some essential element such as K and the synthesis of proteins involved in photosynthetic apparatus and C-metabolism, some mechanisms were specific for each considered metal. Indeed, the kinetic of Cd and Zn accumulation and distribution in leaves, their impact on some specific mineral element distribution, on the leaf morphology, as well as on the importance of some metabolic pathways clearly differ. Indeed, in response to Cd, *Z. fabago* concentrated Cd ions in less metabolic active tissues with a binding to non-protein thiol compounds, and limited water depletion through a reduction in leaf area and transpiration. In response to Zn, the species accumulated Zn ions in larger amount in the less photosynthetically active spongy mesophyll, increased abundance of proteins involved in energy production, and responded to secondary water stress with the synthesis of osmo-protecting compounds and a higher instantaneous water use efficiency compared with the one observed in response to Cd treatment.

ACKNOWLEDGMENTS

This work was supported by the Fonds National de la Recherche Scientifique (FNRS-Belgium, convention n°2.4565.02), by the Wallonnie-Bruxelles International (Bilateral cooperation with Slovenia 2010–2012, Axe 2 – Rech/Ens.sup., project n°13), by the European Community as an Integrating Activity 'Support of Public and Industrial Research Using Ion Beam Technology (SPIRIT)' under EC contract no. 227012, and by the European Synchrotron Radiation Facility (ESRF), Grenoble, France, for provision of synchrotron radiation facilities (project EC 398) and financial support for some of the users. The authors are grateful to Dr. M. Vaccari for assistance in using beamline BM29, to Mrs A. Iserentant, Mrs B. Van Pee and Mrs A. Igosse for their precious technical assistance, and to Mr A. Robledo Miras and Ir. E. Correal for their help in collecting the seeds. The authors also thank the Bureau d'Etudes Environnement et Analyses (BEAGx, Gembloux, Belgium) for soil analyses.

REFERENCES

Ahsan N., Renaut J. & Komatsu S. (2009) Recent developments in the application of proteomics to the analysis of plant responses to heavy metals. *Proteomics* **9,** 2602–2621.

Aidid S.B. & Okamoto H. (1993) Response of elongation growth rate; turgor pressure and cell wall extensibility of stem cells of *Impatiens balsamina* to lead, cadmium and zinc. *Biometals* **6,** 245–249.

Alloway B.J. & Steinnes E. (1999) Anthropogenic additions of cadmium to soils. In *Cadmium in Soils and Plants* (eds M.J. McLaughlin & B.R. Singh), pp. 97–123. Kluwer Academic Publishers, Dordrecht.

Bajji M., Kinet J.M. & Lutts S. (1998) Salt stress effects on roots and leaves of *Atriplex halimus* L. and their corresponding callus cultures. *Plant Science* **137,** 131–142.

Bates L.S., Waldren R.P. & Teare I.D. (1973) Rapid determination of free proline for water-stress studies. *Plant and Soil* **39,** 205–207.

Broadley M.R., White P.J., Hammond J.P., Zelko I. & Lux A. (2007) Zinc in plants. *New Phytologist* **173,** 677–702.

Cakmak I. (2005) The role of potassium in alleviating detrimental effects of abiotic stresses in plants. *Journal of Plant Nutrition and Soil Sciences* **168,** 521–530.

Callahan D.L., Baker A.J.M., Kolev S.D. & Wedd A.G. (2006) Metal ion ligands in hyperaccumulating plants. *Journal of Biological Inorganic Chemistry* **11,** 2–12.

Cestone B., Vogel-Mikuš K., Quartacci M.F., Rascio N., Pongrac P., Pelicon P., . . . Navari-Izzo F. (2012) Use of micro-PIXE to determine spatial distribu-

tions of copper in *Brassica carinata* plants exposed to $CuSO_4$ or CuEEDS. *Science of the Total Environment* **427–428,** 339–346.

Cherif J., Derbel N., Nakkach M., Bergmann H.V., Jemal F. & Lakhdar Z.B. (2010) Analysis of *in vivo* chlorophyll fluorescence spectra to monitor physiological state of tomato plants growing under zinc stress. *Journal of Photochemistry and Photobiology B: Biology* **101,** 332–339.

Conesa H.M., Faz A. & Arnaldos R. (2006) Heavy metal accumulation and tolerance in plants from mine tailings of the semiarid Cartagena-La Union mining district (SE Spain). *Science of the Total Environment* **366,** 1–11.

Conesa H.M., Faz A. & Arnaldos R. (2007) Initial studies for the phytostabilization of a mine tailing from the Cartagena-La Union Mining District (SE Spain). *Chemosphere* **66,** 38–44.

Deinlein U., Weber M., Schmidt H., Rensch S., Trampczynska A., Hansen T.H., . . . Clemens S. (2012) Elevated nicotianamine levels in *Arabidopsis halleri* roots play a key role in zinc hyperaccumulation. *The Plant Cell* **24,** 708–723.

Farinati S., DalCorso G., Bona E., Corbella M., Lampis S., Cecconi D., . . . Furini A. (2009) Proteomic analysis of *Arabidopsis halleri* shoots in response to the heavy metals cadmium and zinc and rhizosphere microorganisms. *Proteomics* **9,** 4837–4850.

Farquhar G.D., Ehleringer J.R. & Hubick K.T. (1989) Carbon isotope discrimination and photosynthesis. *Annual Review of Plant Physiology and Plant Molecular Biology* **147,** 87–92.

Feller U., Anders I. & Demirevska K. (2008) Degradation of Rubisco and other chloroplast proteins under abiotic stress. *General and Applied Plant Physiology* Special Issue **34,** 5–18.

Fukao Y., Ferjani A., Tomioka R., Nagasaki N., Kurata R., Nishimori Y., . . . Maeshima M. (2011) iTRAQ analysis reveals mechanisms of growth defects due to excess Zn in Arabidopsis. *Plant Physiology* **155,** 1893–1907.

Gallego S.M., Pena L.B., Barcia R.A., Azpilicueta C.E., Iannone M.F., Rosales E.P., . . . Benavides M.P. (2012) Unravelling cadmium toxicity and tolerance in plants: insight into regulatory mechanisms. *Environmental and Experimental Botany* **83,** 33–46.

Garcia J.S., Souza G.H.M., Eberlin M.N. & Arruda M.A.Z. (2009) Evaluation of metal-ion stress in sunflower (*Helianthus annuus* L.) leaves through proteomic changes. *Metallomics* **1,** 107–113.

Ghelis T., Dellis O., Jeannette E., Bardat F., Miginiac E. & Sotta B. (2000) Abscisic acid plasmalemma perception triggers a calcium influx essential for RAB18 gene expression in *Arabidopsis thaliana* suspension cells. *FEBS Letters* **483,** 67–70.

Harding M.M. (2001) Geometry of metal–ligand interactions in proteins. *Acta Crystallographica Section D: Biological Crystallography* **57,** 401–411.

Haydon M.J., Kawashi M., Wirtz M., Hillmer S., Hell R. & Krämer U. (2012) Vacuolar nicotianamine has critical and distinct roles under iron deficiency and for zinc sequestration in *Arabidopsis*. *The Plant Cell* **24,** 724–737.

Hossain Z., Hajika M. & Komatsu S. (2012) Comparative proteome analysis of high and low cadmium accumulating soybeans under cadmium stress. *Amino Acids* **43,** 2393–2416.

Hubick K.T., Farquhar G.D. & Shorter R. (1986) Correlation between water-use efficiency and carbon isotope discrimination in diverse peanut (*Arachis*) germplasm. *Autralian Journal of Plant Physiology* **13,** 803–816.

Huguet S., Bert V., Laboudigue A., Barthès V., Isaure M.P., Llorens I., . . . Sarret G. (2012) Cd speciation and localization in the hyperaccumulator *Arabidopsis halleri*. *Environmental and Experimental Botany* **82,** 54–65.

Isaure M.P., Fayard B., Sarret G., Pairis S. & Bourguignon J. (2006) Localization and chemical forms of cadmium in plant samples by combining analytical electron microscopy and X-ray spectromicroscopy. *Spectrochimica Acta – Part B Atomic Spectroscopy* **61,** 1242–1252.

Ishida H., Makino A. & Mae T. (1999) Fragmentation of the large subunit of ribulose-1,5-bisphosphate carboxylase by reactive oxygen species occurs near Gky-329. *The Journal of Biological Chemistry* **274,** 5222–5226.

Kabata-Pendias A. & Pendias H. (2001) Zinc. In *Trace Elements in Soils and Plants* (eds A. Kabata-Pendias & H. Pendias), pp. 131–142. CRC Press, Boca Raton, FL, USA.

Kieffer P., Dommes J., Hoffmann L., Hausman J.F. & Renaut J. (2008) Quantitative changes in protein expression of cadmium-exposed poplar plants. *Proteomics* **8,** 2514–2530.

Kieffer P., Planchon S., Oufir M., Ziebel J., Dommes J., Hoffmann L., . . . Renaut J. (2009) Combining proteomics and metabolite analyses to unravel cadmium stress-response in poplar leaves. *Journal of Proteome Research* **8,** 400–417.

Koren Š., Arčon I., Kump P., Nečemer M. & Vogel-Mikuš K. (2013) Influence of $CdCl_2$ and $CdSO_4$ supplementation on Cd distribution and ligand environment in leaves of the Cd hyperaccumulator *Noccaea* (*Thlaspi*) *praecox*. *Plant and Soil* **370,** 125–148.

Küpper H., Lombi E., Zhao F.-J. & McGrath S.P. (2000) Cellular compartmentation of cadmium and zinc in relation to other elements in the hyperaccumulator *Arabidopsis halleri*. *Planta* **212,** 75–84.

Lefèvre I., Gratia E. & Lutts S. (2001) Discrimination between the ionic and osmotic components of salt stress in relation to free polyamine level in rice (*Oryza sativa*). *Plant Science* **161,** 943–952.

Lefèvre I., Correal E. & Lutts S. (2005) Cadmium tolerance and accumulation in the noxious weed *Zygophyllum fabago*. *Canadian Journal of Botany* **83,** 1655–1662.

Lefèvre I., Correal E., Faz-Cano Á., Zanuzzi A. & Lutts S. (2009) Structural development, water status, pigment concentrations, and oxidative stress of *Zygophyllum fabago* seedlings in relation to cadmium distribution in the shoot organs. *International Journal of Plant Sciences* **170,** 226–236.

Lefèvre I., Correal E. & Lutts S. (2010a) Impact of cadmium and zinc on growth and water status of *Zygophyllum fabago* in two contrasting metallicolous populations from SE Spain: comparison at whole plant and tissue level. *Plant Biology* **12,** 883–894.

Lefèvre I., Marchal G., Ghanem M.E., Correal E. & Lutts S. (2010b) Cadmium has contrasting effects on polyethylene glycol ? Sensitive and resistant cell lines in the Mediterranean halophyte species *Atriplex halimus*. *Journal of Plant Physiology* **167,** 365–374.

Li Q., Lau A., Morris T.J., Guo L., Fordyce C.B. & Stanley E.F. (2004) A syntaxin 1, $G\alpha_o$, and N-type calcium channel complex at a presynaptic nerve terminal: analysis by quantitative immunocolocalization. *Journal of Neuroscience* **24,** 4070–4081.

Lichtenthaler H.K. (1987) Chlorophylls and carotenoids – pigments of photosynthetic biomembranes. *Methods in Enzymology* **148,** 350–382.

Lobinski R., Moulin C. & Ortega R. (2006) Imaging and speciation of trace elements in biological environment. *Biochimie* **88,** 1591–1604.

Lombi E. & Susini J. (2009) Synchrotron-based techniques for plant and soil science: opportunities, challenges and future perspectives. *Plant and Soil* **320,** 1–35.

Lombi E., Scheckel K.G. & Kempson I.M. (2011) *In situ* analysis of metal(oid)s in plants: state of the art and artefacts. *Environmental and Experimental Botany* **72,** 3–17.

Marschner H. (1995) *Mineral Nutrition of Higher Plants* 2nd edn. Academic Press, San Diego, CA, USA.

Monnet F., Vaillant N., Vernay P., Coudret A., Sallanon H. & Hitmi A. (2001) Relationship between PSII activity, CO_2 fixation, and Zn, Mn and Mg contents of *Lolium perenne* under zinc stress. *Journal of Plant Physiology* **158,** 1137–1144.

Nagajyoti P.C., Lee K.D. & Sreekanth T.V.M. (2010) Heavy metals, occurrence and toxicity for plants: a review. *Environmental Chemistry Letters* **8,** 199–216.

Nakano R., Ishida H., Makino A. & Mae T. (2006) *In vivo* fragmentation of the large subunit of ribulose-1,5-bisphosphate carboxylase by reactive oxygen species in an intact leaf of cucumber under chilling-light conditions. *The Plant Cell* **47,** 270–276.

Nečemer M., Kump P., Ščančar J., Jaćimović R., Simčič J., Pelicon P., . . . Vogel-Mikuš K. (2008) Application of X-ray fluorescence analytical techniques in phytoremediation and plant biology studies. *Spectrochimica Acta* **63,** 1240–1247.

Page A.L., Miller R.H. & Keeney D.R. (1982) *Methods of Soil Analysis, Part 2 – Chemical and Microbiological Properties* 2nd edn. American Society of Agronomy, Madison, WI, USA.

Pallon J., Auzelyte V., Elfman M., Garmer M., Kristiansson P., Malmqvist K., . . . Wegdén M. (2004) An off-axis STIM procedure for precise mass determination and imaging. *Nuclear Instruments and Methods in Physics Research Section B: Beam Interactions with Materials and Atoms* **219–220,** 988–993.

Perfus-Barbeoch L., Leonhardt N., Vavasseur A. & Forestier C. (2002) Heavy metal toxicity: cadmium permeates through calcium channels and disturbs the plant water status. *The Plant Journal* **32,** 539–548.

Pietrini F., Iannelli M.A., Pasqualini S. & Massacci A. (2003) Interaction of cadmium with glutathione and photosynthesis in developing leaves and chloroplasts of *Phragmites australis* (Cav.) Trin. Ex Steudel. *Plant Physiology* **133,** 829–837.

Pongrac P., Vogel-Mikuš K., Vavpetič P., Tratnik J., Regvar M., Simčič J., . . . Pelicon P. (2010) Cd induced redistribution of elements within leaves of the Cd/Zn hyperaccumulator *Thlaspi praecox* as revealed by micro-PIXE. *Nuclear Instruments and Methods in Physics Research, Section B: Beam Interactions with Materials and Atoms* **268,** 2205–2210.

Poschenrieder C. & Barceló J. (1999) Water relations in heavy metal stressed plants. In *Heavy Metal Stress in Plants, from Molecules to Ecosystems* (eds M.N.V. Prasad & J. Hagemeyer), pp. 207–229. Springer Verlag, Berlin, Germany.

Remans T., Opdenakker K., Guisez Y., Carleer R., Schat H., Vangronsveld J. & Cuypers A. (2012) Exposure of *Arabidopsis thaliana* to excess Zn reveals a Zn-specific oxidative stress signature. *Environmental and Experimental Botany* **84,** 61–71.

Renaut J., Hausman J.F., Bassett C., Artlip T., Cauchie H.M., Witters E. & Wisniewski M. (2008) Quantitative proteomic analysis of short photoperiod and low-temperature responses in bark tissues of peach (*Prunus persica* L. Batsch). *Tree Genetics and Genomes* **4,** 589–600.

Ryan C.G. (2000) Quantitative trace element imaging using PIXE and the nuclear microprobe. *International Journal of Imaging Systems and Technology* **11,** 219–230.

Salisbury E.J. (1927) On the causes and ecological significance of stomatal frequency, with special reference to woodland flora. *Philosophical Transactions of the Royal Society of London. Series B: Biological Sciences* **216,** 1–65.

Sarret G., Saumitou-Laprade P., Bert V., Proux O., Hazemann J.L., Traverse A., . . . Manceau A. (2002) Forms of zinc accumulated in the hyperaccumulator *Arabidopsis halleri*. *Plant physiology* **130,** 1815–1826.

Sarry J.E., Kuhn L., Ducruix C., Lafaye A., Junot C., Hugouvieux V., . . . Bourguignon J. (2006) The early responses of *Arabidopsis thaliana* cells to cadmium exposure explored by protein and metabolite profiling analyses. *Proteomics* **6,** 2180–2198.

Schuler M., Rellán-Álvarez R., Fink-Straube C., Abadía J. & Bauer P. (2012) Nicotianamine functions in the phloem-based transport of iron to sink organs, in pollen development and pollen tube growth in *Arabidopsis*. *The Plant Cell* **24,** 2380–2400.

Semane B., Dupae J., Cuypers A., Noben J.P., Tuomainen T., Tervahauta A., . . . Vangronsveld J. (2010) Leaf proteome responses of *Arabidopsis thaliana* exposed to mild cadmium stress. *Journal of Plant Physiology* **167,** 247–254.

Sharkey T.D. (2012) Mesophyll conductance: constraint on carbon acquisition by C3 plants. *Plant, Cell & Environment* **35,** 1881–1883.

Siddiqui M.H., Al-Waibi M.H., Sakran A.M., Basalah M.O. & Ali H.M. (2012) Effect of calcium and potassium on antioxidant system of *Vicia faba* L. under cadmium stress. *International Journal of Molecular Sciences* **13,** 6604–6619.

Terzano R., Al Chami Z., Vekemans B., Janssens K., Miano T. & Ruggiero P. (2008) Zinc distribution and speciation within rocket plants (*Eruca vesicaria* L. *Cavalieri*) grown on a polluted soil amended with compost as determined by XRF microtomography and micro-XANES. *Journal of Agriculture and Food Chemistry* **56,** 3222–3231.

Trampczynska A., Küpper H., Meyer-Klaucke W., Schmidt H. & Clemens S. (2010) Nicotianamine forms complexes with Zn(II) *in vivo*. *Metallomics* **2,** 57–66.

Van Assche F. & Clijsters H. (1990) Effects of metals on enzyme-activity in plants. *Plant, Cell & Environment* **13,** 195–206.

Villiers F., Ducruix C., Hugouvieux V., Jarno N., Ezan E., Garin J., . . . Bourguignon J. (2011) Investigating the plant response to cadmium exposure by proteomic and metabolomic approaches. *Proteomics* **11,** 1650–1663.

Vogel-Mikuš K., Regvar M., Mesjasz-Przybyłowicz J., Przybyłowicz W.J., Simčič J., Pelicon P. & Budnar M. (2008a) Spatial distribution of cadmium in leaves of metal hyperaccumulating *Thlaspi praecox* using micro-PIXE. *New Phytologist* **179,** 712–721.

Vogel-Mikuš K., Simčič J., Pelicon P., Budnar M., Kump P., Nečemer M., . . . Regvar M. (2008b) Comparison of essential and non-essential element distribution in leaves of the Cd/Zn hyperaccumulator *Thlaspi praecox* as revealed by micro-PIXE. *Plant, Cell & Environment* **31,** 1484–1496.

Vogel-Mikuš K., Arčon I. & Kodre A. (2010a) Complexation of cadmium in seeds and vegetative tissues of the cadmium hyperaccumulator *Thlaspi praecox* as studied by X-ray absorption spectroscopy. *Plant and Soil* **331,** 439–451.

Vogel-Mikuš K., Kump P., Nečemer N., Pelicon P., Arčon I., Pongrac P., . . . Regvar M. (2010b) Quantitative analyses of trace elements in environmental samples: options and (im)possibilities. In *Soil Heavy Metals, Soil Biology*, Vol. **19** (eds I. Sherameti & A. Varma), pp. 113–138. Springer-Verlag, Berlin, Heidelberg.

Vromman D., Flores-Bavestrello A., Šlejkovec Z., Lapaille S., Teixeira-Cardoso C., Briceño M., . . . Lutts S. (2011) Arsenic accumulation and distribution in relation to young seedling growth in *Atriplex atacamensis* Phil. *Science of the Total Environment* **412–413,** 286–295.

Warren C.R. (2008) Stand aside stomata, another actor deserves centre stage: the forgotten role of the internal conductance to CO_2 transfer. *Journal of Experimental Botany* **59,** 1475–1487.

Wehr J.B., Menzies N.W. & Blamey F.P.C. (2004) Inhibition of cell-wall autolysis and pectin degradation by cations. *Plant Physiology and Biochemistry* **42,** 485–492.

Yemm E.W. & Willis J. (1954) The estimation of carbohydrates in plant extracts by anthrone. *Biochemical Journal* **57,** 508–514.

Yuan Q.H., Shi G.X., Zhao J., Zhang H. & Xu Q.S. (2009) Physiological and proteomic analyses of *Alternanthera philoxeroides* under zinc stress. *Russian Journal of Plant Physiology* **56,** 495–502.

Zeng X.-W., Qiu R.-L., Ying R.-R., Tang Y.-T., Tang L. & Fang X.-H. (2011) The differentially-expressed proteome in Zn/Cd hyperaccumulator *Arabis paniculata* Franch. in response to Zn and Cd. *Chemosphere* **82,** 321–328.

Zhao F.J., Lombi E., Breedon T. & McGrath S.P. (2000) Zinc hyperaccumulation and cellular distribution in *Arabidopsis halleri*. *Plant, Cell & Environment* **23,** 507–514.

Received 18 February 2013; received in revised form 20 October 2013; accepted for publication 21 October 2013

SUPPORTING INFORMATION

Additional Supporting Information may be found in the online version of this article at the publisher's web-site:

Figure S1. Scanning transmission ion microscopy (STIM) image and quantitative elemental maps of K, Mg, P, S, Cu, Fe, Mn, Zn, Ca and Cl generated with GEOPIXE II software package after micro-PIXE analysis in a selected area (upper epidermis and mesophyll) of a leaf cross section of *Zygophyllum fabago*. Scan size, 165 μm × 165 μm.

Figure S2. Elemental co-localization in the leaf cross section of *Zygophyllum fabago* after 28 d of 50 μM Zn treatment presented in Fig. 3 [Zn (red) – K (green), – Mg (green), – P (green), – S(green), Cu (green), Fe (green), Mn (green), Ca (green), Cl (green); Ca (red) – Mg (green), – S (green); Mg (red) – S (green), white areas represent overlapping of red and green channels]. Analysis was performed using ImageJ software with the 'intensity correlation analysis' plug-in, generating Pearson's correlation coefficients (r), Mander's overlap coefficients (R) and Intensity Correlation Quotient (ICQ) as detailed in Material and Methods.

Table S1. All the data obtained for the identification of the 67 spots that had a P-value < 0.05 in the two-way ANOVA.